DI-CNG injector nozzle design influence on SI engine standard emissions and particulates at different injection timings

Fuel 317 (2022) 123386

Contents lists available at ScienceDirect

Fuel

journal homepage: www.elsevier.com/locate/fuel

DI-CNG injector nozzle design influence on SI engine standard emissions and particulates at different injection timings

Mindaugas Melaika [a,*], Gilles Herbillon [b], Petter Dahlander [a]

[a] Chalmers University of Technology, Hörsalsvägen 7A, Gothenburg 412 96, Sweden
[b] GDTech Engineering, Avenue de l'Expansion 7, Alleur 4432, Belgium

ARTICLE INFO

Keywords:
Spark ignition engine
CNG direct injection
Biogas
Nozzle head design
Standard emissions and particulates

ABSTRACT

Compressed natural gas direct injection (DI-CNG) systems in spark ignition (SI) internal combustion engines have shown that it can give several benefits compared to CNG port fuel injection systems. However, the DI-CNG injector nozzle head design and gas jet formation may greatly influence engine exhaust gas emissions and performance. Present experimental study investigated the influence of 7 different nozzle head designs of spray-guided DI-CNG injectors on the combustion process, engine performance, standard emissions, and particulate number (PN) when methane fuel was injected at different injection timings (SOI) and injection pressures (18 bar and 50 bar). The nozzle heads had two main design patterns – heads with small multi holes/orifices and heads with larger crevices (swirl or umbrella spray pattern). Naturally aspirated SI engine tests were conducted at part load (6 bar IMEP) and wide-open throttle (WOT) at 2000 rpm engine speed. The results revealed that the difference between the nozzle heads was small when the fuel was injected at an early stage of the intake stroke (310–350 CAD bTDC) either at part load or high load. However, for late injection timing (130–190 CAD bTDC), the design of the DI-CNG injector nozzle head had a large impact on the combustion stability, standard emissions formation and particulates. Multi-hole nozzle heads showed improved CO_2, CO, THC, total PN, and slightly higher NO_x emissions compared to nozzle heads with larger crevices. For some of the nozzles, the SOI could be retarded more than for other injector head designs at higher injection pressure whilst still ensuring an acceptable engine performance in terms of combustion stability, power output and emissions formation. Overall, 50-bar injection pressure and a late injection timing under WOT conditions achieved higher engine load levels with all injector nozzle types. Images acquired using an optical endoscope technique with a high-speed video camera showed that a yellow flame was present for all nozzle types at a low injection pressure and late SOI. Increasing the injection pressure reduced the injection duration, improved air/fuel mixing which resulted in the reduced yellow flame formation and lower PN for most of the nozzle heads.

1. Introduction

Improving the air quality (via a decrease of greenhouse gases emissions – GHG) and reducing the dependency on fossil fuels (via quantification of CO_2 emissions) are the main priorities of the worldwide regulation organizations while setting new rules for the transport industry.

For example, Europe's transport sector is responsible for ~25% of GHG emissions and is still growing. However, it is estimated that a reduction of transport emissions of 90% is needed to achieve climate neutrality aimed for by 2050 [1]. Most ground vehicles still use internal combustion engines (ICEs) running on fossil fuel. One of the ways to reduce tank-to-wheel CO_2 emissions and other hazardous emissions is to reduce the dependency on fossil fuel and develop vehicles that can run on renewable biofuels (e.g., biodiesel, biogas, bioethanol) or carbon-free fuels (e.g., hydrogen). One of the most promising technologies is electric vehicles. However, the shift toward electrification is challenging globally. Therefore, vehicles powered by ICEs are still expected to be present as long as they will comply with emission standards. The EU has set a target to reach 20% electric vehicles, 40% hybrid vehicles (HEVs), 30% conventional vehicles and 10% fuel cell electric vehicles (FCEVs) by 2030, which could reduce CO_2 emissions from passenger vehicles by 70% [2]. Since ICEs are still the main solution for medium and heavy-duty trucks, off-road vehicles and marine applications, efforts must be made to improve the ICE efficiency and reduce the CO_2 footprint.

* Corresponding author.
E-mail addresses: melaika@chalmers.se (M. Melaika), gilles.herbillon@gdtech.eu (G. Herbillon), dallas@chalmers.se (P. Dahlander).

https://doi.org/10.1016/j.fuel.2022.123386
Received 3 November 2021; Received in revised form 31 December 2021; Accepted 19 January 2022
Available online 3 February 2022

Nomenclature

A/F	air/fuel ratio
aTDC	after top dead center
bTDC	before the top dead center
BDC	bottom dead center
CA10-90	crank angle degrees between 10% and 90% of burned fuel
CAD	crank angle degree
CH_4	methane
CNG	compressed natural gas
CoV	coefficient of variance
CR	compression ratio
DI	direct injection
H_2	hydrogen
H/C	hydrogen and carbon ratio
ICE	internal combustion engine
IMEP	indicated mean effective pressure
iSFC	indicated specific fuel consumption
iSCO	indicated specific carbon monoxide emissions
$iSCO_2$	indicated specific carbon dioxide emissions
iSHC	indicated specific hydrocarbon emissions
$iSNO_x$	indicated specific nitrous oxide emissions
LHV	lower heating value
MBT	maximum brake torque
MFB50	50% of burned fuel mass
MN	methane number
PAH	polycyclic aromatic hydrocarbons
PFI	port fuel injection
PN	particulate number
rpm	revolutions per minute
SI	spark ignition
SOI	start of injection
ST	spark timing
THC	total hydrocarbons
WOT	Wide-open throttle
λ	Lambda

Improvements in ICEs can be achieved in several ways. One way is to apply different technical solutions for the engine, e.g., variable compression ratio, higher fuel injection pressures, improved ignition systems, engine downsizing, Miller cycle, etc. Another way is to apply low carbon fuels or carbon-free fuels for presently developed and new generation engines. One of the quickest solutions to decrease CO_2 emissions from ICEs by at least 20% is to utilize the methane-based fuel compressed natural gas (CNG) [3]. Biogas and biomethane also contain methane as the main component, and these renewable fuels can be mixed with CNG. The methane (CH_4) molecule comprises just 1 atom of carbon and 4 atoms of hydrogen. As the number of chains between methane and hydrogen is smaller, the combustion generates less unburned gases and lower CO_2 emissions compared to other standard fuels, e.g., gasoline and diesel. A recent comparison between liquified petrol gas (LPG) and CNG revealed that the use of CNG can achieve lower CO_2 and CO emissions [4]. Also, CNG engines can reach a lower brake specific fuel consumption (BSFC) and lower other emissions, e.g., hydrocarbons (HCs) and carbon monoxide (CO) [5,6]. However, natural gas is still a fossil fuel. Thus, biogas and biomethane are more desirable as these fuels can be produced from different waste sources. Biogas usually contains a high concentration of CO_2 and other dilutants. Biomethane is obtained after cleaning biogas and contains a high concentration of methane. It can be compressed, mixed with natural gas or directly applied for different vehicle types (light-duty or heavy-duty).

Many experimental studies have demonstrated that the use of methane-based fuels can reduce standard emissions. Some studies have also investigated soot formation and particulate number (PN) emissions from CNG engines. CNG can generate low amounts of volatile organic compounds (VOCs) and particulates due to the simple chemical composition of methane. However, particulate formation in CNG engines may still be an issue [7]. It has been shown that a CNG engine equipped with a port fuel injection (PFI) system can achieve lower PN values compared to gasoline and diesel cases [8]. Measurements of a CNG heavy-duty engine during a World Harmonized Transient Cycle (WHTC) showed that most of the particulates were $\leq$ 23 nm in diameter. It has been suggested that engine oil is one of the main sources of particulates [9,10]. Comparison of CNG (PFI), CNG/H_2 mixture (PFI), gasoline (PFI) and diesel (direct injection, DI) fuels showed that for CNG and CNG/hydrogen fuels, PN peaked in the nuclei mode size range, which was attributed to incomplete combustion of lubricating oil. Hydrogen addition to natural gas has been shown to improve combustion and reduce soot formation precursors (HCs and polycyclic aromatic hydrocarbons, PAHs), resulting in even lower PN emissions [11].

Present vehicles running on methane-based fuels usually have PFI-CNG systems, which are relatively inexpensive, reliable and easily fitted in the engine. Also, such systems can achieve a high level of air/fuel homogeneity [12]. However, the use of PFI-CNG systems may be hampered by several issues. CNG fuel injected into the air intake manifold occupies some of the available volume, which affects the engine's volumetric efficiency and reduces the engine power output [5,13].

One of the ways to improve engine performance for gaseous fuels is to apply a DI-CNG system. However, the technology is not yet applied in mass vehicle production. DI-CNG can allow a gaseous fuel to be injected into the cylinder at different injection timings. The volumetric efficiency is increased when gaseous fuel is injected at the end of the intake stroke or after the intake valves are closed. Different experimental and numerical investigations have concluded that the start of injection (SOI) has a large impact on various engine parameters, e.g., power output and emissions. Tests at part loads have shown that late injection after intake valve closure in a natural gas DI engine significantly increases the combustion rate [14]. Under wide-open throttle (WOT) conditions, the late injection has been shown to increase the volumetric efficiency and work output [14]. The use of late SOI timing in a DI system, increases the energy density of gaseous fuels, increasing the volume of air and improving the volumetric efficiency [15]. It has been demonstrated that the volumetric efficiency for a DI-CNG system and late injection timing can be increased by 9.5% [16]. Other studies have shown that late injection timings can increase the cylinder peak pressure, power and torque and achieve lower BSFC [17]. However, the maximum brake torque (MBT) may decrease at high engine speed when fuel is injected later due to limitations in air/fuel mixing and the possible injection duration window. Late injections require later spark timing to obtain sufficient air/fuel mixing [15]. On the other hand, the use of high injection pressure and late injection timing in DI-CNG can increase the indicated mean effective pressure (IMEP) compared to early injection timing, especially under lean combustion conditions. One of the main conclusions of these studies is that late high-pressure injection accelerates methane combustion [16].

Recent experiments and simulations of liquid fuels carried out by industry and academia showed that various DI injector parameters, e.g. high injection pressure, nozzle hole designs, fuel spray line distribution, can greatly influence the liquid fuel combustion process and exhaust gas emissions formation [18,19,20,21]. Gaseous fuels, e.g., natural gas, methane and biogas, do not need to be evaporated when injected into the engine which is one of their main advantages compared to liquid fuels (e.g., gasoline, diesel, ethanol, methanol). Also, gaseous fuels do not create wall-wetting on the piston and on the combustion chamber or

cylinder walls. However, several characteristics can affect the gas jet and its mixing with air in the cylinder. Gaseous fuel injection behaves differently from that of liquid fuel as gaseous fuels have a lower jet momentum to impose motion of the mixture or support mixing through jet impingement. Usually, a lower injection pressure is preferable for DI-CNG systems, corresponding to lower gas jet momentum [22]. It has been shown that in gas jets, the flow is complex and shock waves and expansion fans significantly affect the mass flow rate and air/fuel mixing [23]. Also, different gases may exhibit different behavior during the injection process. Methane gas, which is the dominant component in CNG, biogas and biomethane fuel, has problems related to penetration length and radial expansion compared to the alternative carbon-free gaseous fuel hydrogen. Comparison between methane and hydrogen jets has shown that under an identical nozzle pressure ratio (NPR) and elevated ambient temperature and pressure, methane generated a much lower penetration length and volumetric growth compared to hydrogen [23]. Methane also exhibited a noticeably lower volumetric growth when the jet was present in cold and hot environments at the same ambient pressure and NPR. These results suggest that methane's relatively lower radial expansion of the jet is due to a lower molecular diffusivity and weak vortex ring [24]. However, the main influence on mixture formation is the DI injector design.

Yosri et al. have demonstrated that NPR and the nozzle geometrical features are the main parameters affecting the fuel mass flow rate and air/fuel mixing [25]. Deshmukh et al. concluded that pressure changes in the cylinder due to the SOI timing and injection pressure influence the injector nozzle operation [26]. The nozzles may work under expanded, perfectly expanded, over expanded or subsonic modes, which can affect the jet velocity. The mixing process is also affected by complex shock structures formed downstream of the nozzle, which are in turn influenced by high-pressure gaseous injection [27]. Experiments have shown that higher injection pressures resulted in higher injection shape symmetry, which was attributed to uneven nozzle opening due to the highly turbulent nature of the flow and randomness associated with radially spreading jets [27]. Because of the uneven symmetry of a low-pressure jet, the homogeneity may be lower in the cylinder compared to higher injection pressures and more symmetrical injections. At higher injection pressures, the jet tip penetration speed is higher [28]. The fuel concentration is also higher [27].

Several investigations have shown that the injector needle's opening design can also have an impact on mixture formation. Gaseous DI injectors can have different needle opening designs, e.g., inwards opening valve or outwards poppet valve. Inwards opening injectors can suffer from gas remaining in the dead volume (located downstream the sealing diameter or valve seat). However, outwards opening injectors may exhibit phenomena of choking, shock waves and boundary layer separation when a compressible gas flows through the small injector passages [25,26]. It has been shown that in an outwards opening poppet valve type injector, the radial expansion distance of injected methane gas increases with increasing injection time and increasing the injection pressure [29]. Swantek et al. highlighted that higher injection pressure shows wider jet [30]. However radial expansion distance can decrease in lower ambient pressure levels [29]. Results showed that the injection pressure did not affect the radial penetration when the fuel was injected under ambient pressure conditions (1 bar). The ambient pressure was the most influencing parameter for radial penetration. It also strongly affected the axial fuel jet penetration. However, the ambient pressure had a larger effect on axial penetration when the injection pressure was increased [29].

Another important parameter for combustible mixture formation is the injector nozzle's head/tip design. Investigation of different nozzles and injection pressures at early and late injection timings has shown that the mixing rate is more sensitive to an injection timing change than to the injection pressure [31]. The results suggested that the mixing mechanism was strongly dependent on nozzle design. The degree of hollow cone nozzle had an impact on homogeneous air/fuel mixture formation. One of the nozzles showed the best results at early SOI timing, whereas another achieved the best results at late injection timing [31]. Simulations of a multi-hole and single-hole injector showed that the multi-hole injector produced a lower amount of fuel-rich mass fraction in the cylinder compared to the single-hole injector. However, the flammable mass fraction was similar for both injectors when the injection was at late timing at the end of compression stroke [32]. Experimental and simulation results have also revealed that nozzles with a larger nozzle diameter show a higher pressure drop due to higher passing momentum [33]. It was noted that the initial pressure drop was greater than the jet pressure steady decrease due to the initial acceleration of the jet. Also, higher pressure ratios between injection and the environment resulted in longer jet penetration. It was observed that the jet diameter affected the available air/fuel mixing time, resulting in fuel-rich zones around the injector nozzle [33]. The injector nozzle head design also influences engine performance and emission formation. DI-CNG experimental tests with nozzles having different spray angles revealed that the design of the injector nozzle can have an impact on iSCO, iSHC and $iSNO_x$ emissions. In particular, some of the nozzles improved the mixing, reduced iSFC or achieved more stable combustion as CoV_{IMEP} was lower [34]. However, Seboldt et al. noted that detailed engine calibration is required for different DI-CNG injector nozzle angles [35]. HC emissions were highest even at an early injection timing (SOI 240 CAD bTDC) due to scavenging. DI system optimization for a gaseous fuel is also important to reduce PN emissions. As mentioned above, PFI-CNG systems usually achieve lower PN emissions. Several DI-CNG system research studies have shown that particulates are mainly present in the nuclei mode particle size range, as for PFI cases [36]. Application of a DI-CNG system in a new generation downsized engine for an ultralight vehicle also demonstrated that PN emissions were at a low level [37]. Variation of the injection timing also enabled low PN emissions with DI-CNG when the fuel was injected during the intake or compression stroke [38].

The above literature clearly shows that the DI-CNG injector nozzle head design, injection pressure and injection timing can have large effects on mixture formation and combustion processes for a given combustion chamber designs, inclination of air intake ducts, injector inclination/positioning. Overviewed literature revealed that investigations related to DI-CNG technology mainly focused on several different areas – investigations about the jet formation in spray chambers (different injection pressures, ambient pressures, injector needle opening type, etc.). Also, a wide variety of engine tests were carried out by different research groups which focused on DI injectors and different injection pressures or injection timings. Some of the researches involved several injector nozzle head/tip configurations. Mentioned engine tests mainly focused on standard emissions rather than PN emissions. There is still a lack of experimental test data and analysis on how different nozzle head designs influence combustible mixture formation, combustion process, engine performance and emissions formation. Especially there is a lack of nozzle head design investigations that involve high-speed video imaging and capturing the combustion process which can give supportive results. Therefore, this study aimed to investigate experimentally a broad spectrum of spray-guided DI-CNG injector nozzle head designs (7 different nozzle head designs) and determine their influence on the combustion process, standard emissions and particulate formation in the same SI single-cylinder engine. The main objectives were to determine how DI-CNG injector nozzle heads, having large crevices or different multi-hole patterns, can influence jet and combustible mixture formation, engine performance and emissions. Also, investigate how these different nozzle heads behave at different engine loads and have an influence on mentioned engine parameters when gaseous fuel is injected at different injection timings and at different injection pressures. Objectives additionally included the high-speed video imaging and endoscope technique application which can support and give additional explanations about emissions formation in the engine.

2. Experimental setup and testing methodology

Experiments were conducted with a single-cylinder spark ignition (SI) engine coupled with an "AVL 5411" engine test bench. Engine setup is presented in Fig. 1, whereas engine technical data is presented in Table 1.

The engine was supplied with an external air supply system (external electric air compressor device) that could create up to a 2 bar air boost in the air intake manifold. The air intake temperature was kept constant at +25 °C. The air supply and control system ensured the acquisition of stable testing data and avoided additional fluctuations that could affect the engine work process. The present study focused solely on naturally aspirated engine conditions. Thus, the maximum air charging to the engine was set to 1 bar.

The test engine had a compression ratio of 10:1, which is usual for a CNG engine having a turbocharging system. The engine had a 4-valve system with an intake and exhaust valve overlap of 23 CAD at 0 mm valve lift for air intake scavenging purposes.

The air intake pressure was adjusted with a throttle valve according to the target air/fuel (A/F) ratio – stoichiometric conditions ($\lambda = 1.0$). Lambda was determined using a lambda sensor mounted in the exhaust pipe which measured the oxygen content. A Horiba Mexa-110 system was used to determine the air/fuel (A/F) ratio according to the fuel H/C atom ratio (accuracy ± 0.70 %). The engine SI system had a single J-gap type electrode spark plug. Spark timings were adjusted for each test point separately to achieve the combustion phasing at 6–8 CAD aTDC for the 50% of mass fuel burned fraction (MFB50).

The injector was the spray-guided type. The injector control voltage settings were the same as those of a standard GDI system, i.e., 65 V to open the injector needle and 12 V to hold the injector open. The injection duration was controlled with a National Instruments Direct Drive System control module. The injector was able to inject the fuel from 18 bar to 50 bar injection pressure depending on the required fuel flow and possible injection duration to achieve the required engine load. Owing to the special injector design, it was possible to change injector nozzle heads.

Photographs of the DI-CNG injector and nozzle heads used are shown in Fig. 2. Experiments were conducted with 7 different nozzle head designs.

Nozzle head 1 had multiple holes (9 holes positioned circularly and 1 centrally). Nozzle head 2 featured a single cone spray design which was able to create a swirl motion in the gas jet. Nozzle heads 3, 4, 5 featured single cone design (without swirl). Nozzle head 6 also had a single cone spray design but with an additional central hole. Nozzle head 7 was designed to create a triple cone jet.

Nozzle heads 1, 5, 6 and 7 were able to spray the gas jet more symmetrically downstream to the cylinder when the injector was mounted centrally in the engine cylinder head. This type of nozzle head was able to split the gas jet into smaller gas jets due to the small holes in the nozzle heads. Nozzle heads 2, 3 and 4 formed a different group that had larger crevices. The spray from nozzle 2 was able to create swirl motion from 3 holes in the head. The nozzle head 3 generated spray with an umbrella-shaped jet. Nozzle head 4 was similar to nozzle head 3 but

Table 1
Engine and injection system specifications.

Parameter	Value
Displaced volume (V_h), [dm^3]	0.5
Stroke (S), [mm]	90.0
Bore (D), [mm]	82.0
Compression ratio (CR), [-]	10:1
Number of valves, [-]	4
Intake air temperature (T_{air}), [°C]	+25
Intake valve opening (IVO)	353 CAD
Intake valve closing (IVC)	606 CAD
Exhaust valve opening (EVO)	112 CAD
Exhaust valve closing (EVC)	375 CAD
Air boosting max, [bar]	2
Injector type	DI, solenoid, inwards opening
Injection type	Spray guided
Injector positioning in the cylinder	0° inclination with piston axis
Control peak/hold, [V]	65/12
Injection pressure, [bar]	18–50

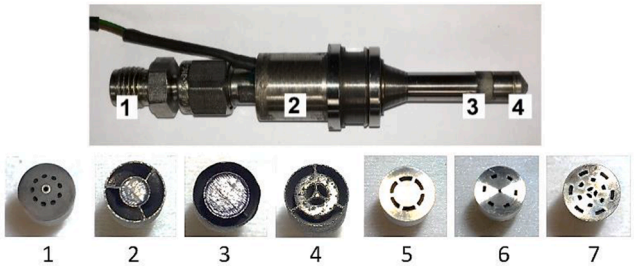

Fig. 2. Photograph of a DI-CNG injector (1 – connection to the gas supply; 2 – solenoid; 3 – injector nozzle; 4 – interchangeable nozzle head) and 7 different nozzle head designs.

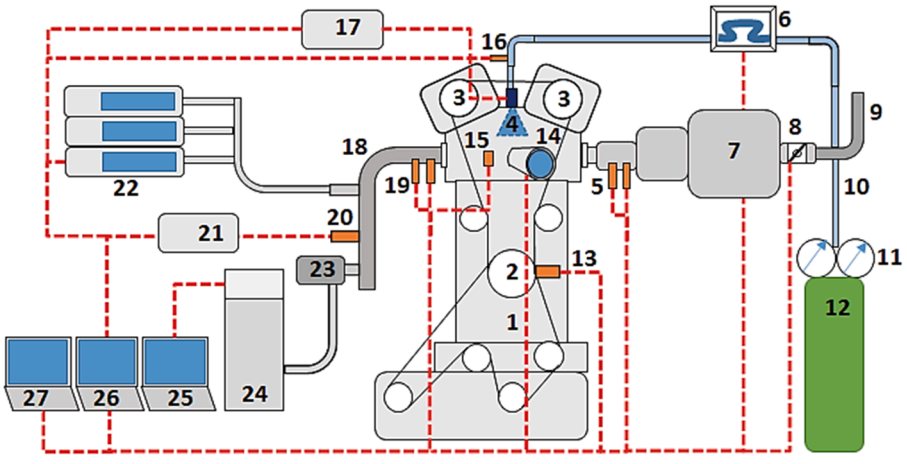

Fig. 1. Test engine system layout: 1 – AVL single-cylinder SI engine; 2 – crankshaft; 3 – camshafts; 4 – GDTech DI-CNG injector; 5 – intake air pressure and temperature sensors; 6 – Micro Motion Elite Coriolis fuel flow meter; 7 – air intake plenum and runners; 8 – throttle valve; 9 – compressed air supply system; 10 – fuel supply line; 11 – gas pressure regulator; 12 – methane gas tank; 13 – AVL 365 crank angle encoder; 14 – LaVision endoscope with Ametec Vision Research Phantom Miro M310 high speed video camera; 15 – AVL GH14DK cylinder pressure sensor; 16 – Kistler 4618A2 gaseous fuel pressure sensor in fuel supply line; 17 – NI Direct Injector Drive System for DI injector control system; 18 – exhaust gas pipe; 19 – exhaust gas pressure and temperature sensors; 20 – lambda sensor; 21 – Horiba Mexa-110 A/F ratio measurement system; 22 – standard emissions analyzers J.U.M. VE7, Fuji Electric ZPA, Eco Physics CLD822 CMhr; 23 – heated sample line for fast particulate analyzer; 24 – Cambustion DMS500 MkII fast particulate analyzer; 25 – fast particulate analyzer data sampling computer; 26 – AVL Indicom and AVL Puma software for engine control and data acquisition; 27 – combustion images sampling computer.

had central holes that could spread the jet centrally and outwards.

Experiments were conducted with 100% methane as fuel, which is the main component of the methane-based fuels CNG, biogas and biomethane. The use of a single component fuel reduced the possibility of opposing effects on various engine measurements, as may occur with multicomponent natural gas fuel. CNG gas quality may have an influence on mixture quality during gas DI injection [39]. Also, 100% methane is close to some of the CNG compositions from specific natural gas suppliers globally [40,41] and the composition of biomethane after biogas is cleaned of impurities and dilutants. The physicochemical properties of methane are presented in Table 3.

Methane gas has a low carbon content and a hydrogen/carbon atom ratio of 4:1. Its lower heating value (50 MJ/kg) based on mass is also higher than other liquid and gaseous fuels. Methane gas was supplied from a pressurized 200 bar bottle fitted with a pressure reducer to achieve the target injection pressure for the DI-CNG injector. The gas flow was measured with a Micro Motion Elite Coriolis mass flow meter CMF010M323NB (accuracy ± 0.35 %).

The cylinder pressure inside the engine cylinder was measured with an AVL GH14DK pressure sensor (sensor sensitivity 19 pC/bar) with a frequency of 170 kHz and accuracy of ± 1.50 %. Pressure values were sampled at 0.1 CAD from 50 CAD bTDC to 90 CAD aTDC. The rest of the range was sampled with a resolution of 1 CAD. A single sample of pressure data consisted of 300 combustion cycles measured continuously. Each testing point was repeated at least 3 times. Thus, a total of at least ~900 combustion cycles were recorded and analyzed. An AVL Indicom system was used for cylinder pressure data acquisition.

Standard emissions were measured with different types of analyzers. CO_2 and CO were measured with a Fuji Electric ZPA gas analyzer based on a non-dispersion infrared method (NDIR). Total hydrocarbon (THC) emissions were measured with a J.U.M. VE7 flame ionization detector (FID). NO_X emissions were measured with an Eco Physics CLD822 CMhr based on chemiluminescence measurement. The exhaust gas was pumped from the engine exhaust gas pipe through a sampling probe and sampling line kept at a temperature of +190 °C to avoid gas condensation. Sampled standard emissions data are presented as g/kWh values. The values are presented as means with error bars showing standard deviations of obtained data. Error bars for some cases are small and lies in a range of data point marker. Measurements of standard emissions at each testing point were sampled for at least 30 s, after which an AVL Puma acquisition system was used to record the average value. Each testing point was recorded at least 3 times.

The experimental investigation included total PN and size distribution measurements acquired with a Cambustion DMS500 MkII fast particle analyzer and an in-built dilution system that could be adjusted to keep the measurement signal strength within certain limits. PN measurement accuracy – ±5.00 % for 5–300 nm size range and <10.0 % for 300–1000 nm range. The diluted gas flow was compensated by the gas analyzer software. A heated sampling line (+150 °C) and probe were connected separately from the standard emissions measurement line. A sampling of PN was carried out at least 3 times for each testing point. Total PN and particle size distribution data are presented with error bars representing the standard deviation.

Visual analysis of the combustion process was also included in the present experiments. The optical setup (Fig. 3) included a LaVision Hybrid Camera endoscope, which was attached to the front of the engine cylinder head to enable visual access into the combustion chamber. Combustion images were captured with an Amatec Vision Research Phantom Miro M310 high-speed color video camera equipped with a Carl Zeiss 85 mm f/2 lens.

Fig. 4 shows the view of the combustion chamber through the endoscope setup, which enabled visual access of the spark plug, injector tip, intake and exhaust valves. Combustion images were recorded when the camera triggered 1 CAD before spark timing CAD. Images were recorded with a 512x464 pixel resolution and exposure time of 49.64 µs. The sample rate was 12,000 frames per second.

The engine testing points and conditions are presented in Table 4. Tests were conducted with 7 different nozzle heads at 2000 rpm engine speed and two load points – part load at 6 bar IMEP and high load at WOT. Presented results did not include the comparison with a standard PFI-CNG system because the main aim of the present research was to have a versatile comparison and analysis of different DI-CNG injector nozzle heads. However, presented results can be compared with the PFI-CNG results which were presented in a previous study where GDI, PFI-CNG and DI-CNG systems were investigated at similar engine operating conditions [42].

Operating conditions were selected according to a previously carried out investigation of different driving cycles (NEDC, WLTC, RTS95) of engine running on different fuels (gasoline, diesel, ethanol, CNG). It was determined that at specific intervals of driving cycles (especially in more aggressive driving cycles – WLTC and RTS95) engine works at part load (6 bar IMEP) or high load (9 bar IMEP) conditions [43]. The part load conditions used 18 bar (low) injection pressure for all nozzle heads. Lower injection pressure is preferable under low part load conditions because of the required lower fuel amount and the possibility to inject the fuel in a stable short injection duration range. The WOT conditions included both 18 bar (low) and 50 bar (high) injection pressure for all 7 nozzle designs. The lower injection pressure (18 bar) was tested at the high load point (WOT) to investigate the possibility and challenges of using a lower injection pressure at high load conditions. A high injection pressure (50 bar) at WOT was tested in order to achieve short injection durations which can ensure sufficient time for air and fuel mixing. 6 bar IMEP tests were conducted at SOI timings from early 350 CAD to late timing at 170–130 CAD bTDC. WOT testing points included SOI timing

Table 3
Physicochemical properties of methane fuel.

Properties	Value
Fuel composition, [$\%_{Vol.}$]	100 % CH_4
Hydrogen (H) %	25
Carbon (C) %	75
H:C ratio	4:1
Density at + 25 °C, [kg/m^3]	0.657
Methane number (MN)	100
Stoichiometric A/F ratio, [kg_{air}/kg_{fuel}]	17.2
Lower heating value, [MJ/kg]	50

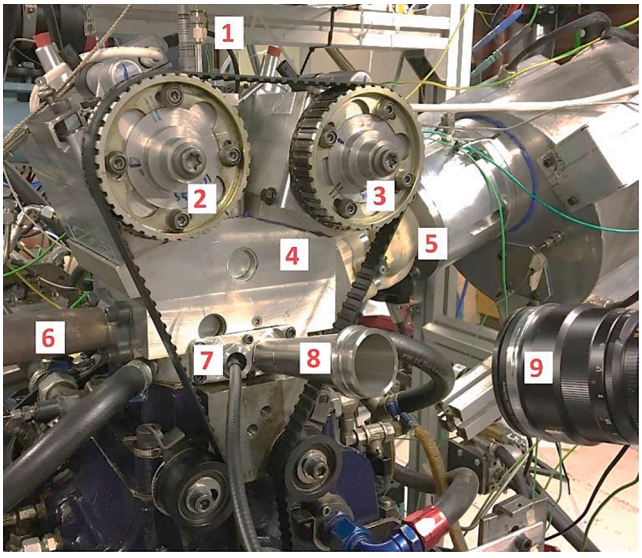

Fig. 3. Optical setup for the single-cylinder test engine: 1 – DI-CNG injector; 2 – exhaust camshaft; 3 – intake camshaft; 4 – cylinder head; 5 – air intake runner; 6 – exhaust gas pipe; 7 – access for LED light; 8 – LaVision endoscope; 9 – Ametec Vision Research Phantom Miro M310 high-speed video camera.

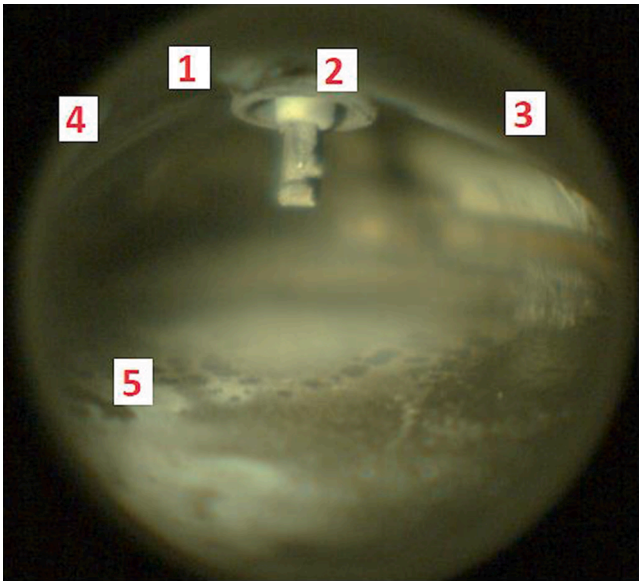

Fig. 4. Combustion chamber image captured through the endoscope: 1 – DI-CNG injector nozzle head; 2 – spark plug; 3 – intake valve; 4 – exhaust valve; 5 – piston surface.

Table 4
Engine operating points for the DI-CNG injector.

Engine speed (*N*), [rpm]	Engine load (IMEP), [bar]	Injection pressure, [bar]	Injection timing (SOI), CAD bTDC	Lambda, [-]
2000	6	18	350–130	1.0
	~8.5–9.5 bar (WOT)	18	310–190	1.0
	~8.5–10 bar (WOT)	50	310–130	1.0

from 310 to 190 CAD bTDC for all nozzles at 18 bar injection pressure and from 310 to 170–130 CAD bTDC at 50 bar injection pressure, depending on the nozzle head design. The latest injection timing depended on the nozzle head design. Retardment of the SOI timing was selected for each nozzle depending on several criteria – decreased combustion stability and increased total PN level close to the limit of the measurement equipment. Additional calculations in a present study to obtain iSFC, CA10-90, CoV_{IMEP} were carried out according to [44], as presented in our previous study [42].

3. Results

3.1. Engine performance

The initial engine performance analysis included results of maximum possible achievable IMEP under WOT conditions. The maximum IMEP values at WOT for two different injection pressures (18 bar and 50 bar) and at different injection timings are presented in Fig. 5.

Initial observations showed that the maximum IMEP level varied depending on the nozzle head type. The difference was especially noticeable at the low injection pressure of 18 bar (Fig. 5a), with nozzle heads 2 and 3 achieving the lowest IMEP over the whole SOI timing range compared with the other nozzle heads. However, the difference in the maximum IMEP between the nozzles decreased when the injection pressure was increased to 50 bar (Fig. 5b).

The results showed that at the lower injection pressure (Fig. 5a), IMEP increased when the fuel was injected at 250 CAD bTDC compared to 310 CAD bTDC. IMEP increased by 2–4.8% depending on the nozzle type when the SOI timing was shifted from 310 to 250 CAD bTDC. The main reason for the increased power output is the fuel was injected later during the intake stroke, which allowed more air into the cylinder.

The highest IMEP values were achieved with nozzle heads 1, 6 and 7. However, further retarding the SOI timing toward 190 CAD bTDC decreased IMEP for all nozzle types. The trends of reduced engine maximum brake torque and load at late injection timings were similar to those observed in other studies. Mohammed et al. showed that a later SOI timing reduced the time between fuel injection and fuel ignition, decreasing the time available for air/fuel mixing and generating a more inhomogeneous mixture in the cylinder [45].

A similar trend of increasing IMEP at increased injection pressure (50 bar) (Fig. 5b) was observed with the different nozzle heads when the SOI timing was shifted from 310 to 250 CAD bTDC. However, IMEP continued to increase when the SOI timing was 190 CAD bTDC, in contrast to the trend observed at 18 bar injection pressure. For some nozzle heads, e.g., 1 and 6, IMEP also increased when the SOI timing was retarded to 170 CAD bTDC. One explanation for the higher IMEP at later timings for 50 bar compared to 18 bar injection pressure is turbulence in the cylinder was increased by a higher injection pressure at later injection timings, improving the combustion process. Other research works also noted that DI-CNG injection can provide additional turbulence energy inside the cylinder when the fuel is injected later [46] which can increase the rate of heat release and achieve faster combustion [47]. Also, at later injection timings the volumetric efficiency was likely improved as more air was present in the cylinder. Choi et al. stated that at late DI-CNG injection timings the charging coefficient increased together with the possible injected mass flow which resulted in an increased in-cylinder pressure and maximum IMEP [48]. In the present study, the increase of IMEP at 190 CAD bTDC was between 7.8% and 9.4% depending on the nozzle type compared to early 310 CAD bTDC injection timing. Injection timings later than 170 CAD bTDC showed a decrease in IMEP for injector nozzle heads 1 and 7. Again, nozzle types 2 and 3 showed the lowest IMEP values over the whole SOI timing range.

The initial analysis revealed that optimization of the nozzle head type, injection pressure and injection timing is important to achieve the best engine performance in terms of power output. The results clearly showed that late injection was beneficial and WOT conditions required a higher injection pressure for late injection timings beyond the bottom dead center (BDC).

CoV_{IMEP} values are presented in Fig. 6 for 6 bar IMEP and WOT conditions (~8.5–10 bar IMEP) for two different injection pressures (18 bar and 50 bar) and different SOI timings. At 6 bar IMEP engine load, CoV_{IMEP} for all the DI-CNG injector nozzle types was below 1.5% when the SOI timing was in the range 350–250 CAD bTDC. When the SOI timing reached 190 CAD bTDC, the CoV_{IMEP} values started to increase for most of the nozzle heads. A sharp increase in CoV_{IMEP} was observed when the SOI timing was later than 180 CAD bTDC. A previous DI-CNG study also showed that the use of a very late injection timing decreased the combustion stability and increased CO and HC emissions [49]. This implies that the combustion process was hampered by a lack of time to mix the air and fuel to achieve a homogeneous mixture, as discussed later.

When the engine load was increased to WOT conditions and the injection pressure was 18 bar (Fig. 6b), the CoV_{IMEP} values were similar to the 6 bar IMEP cases from 310 CAD to 250 CAD bTDC. Later timing increased CoV_{IMEP}. However, the stability was decreased at earlier SOI timings (between 250 CAD bTDC and 190 CAD bTDC) than for 6 bar IMEP conditions. Comparison of the same late injection timing (190 CAD bTDC) at 6 bar IMEP and 9 bar IMEP load showed that for some of the nozzle designs, CoV_{IMEP} was in the range of 5% to 10–15%. For example, nozzle head 5 did not achieve stable combustion at 200 CAD bTDC under WOT conditions. The high CoV_{IMEP} issue at late injection timing was mainly related to the high load and demand to inject a high amount of gaseous fuel, which possibly was not able to mix with air properly before ignition. Nozzle heads 2, 3 and 4 showed higher CoV_{IMEP} values than the other nozzle types for both load conditions, whereas the

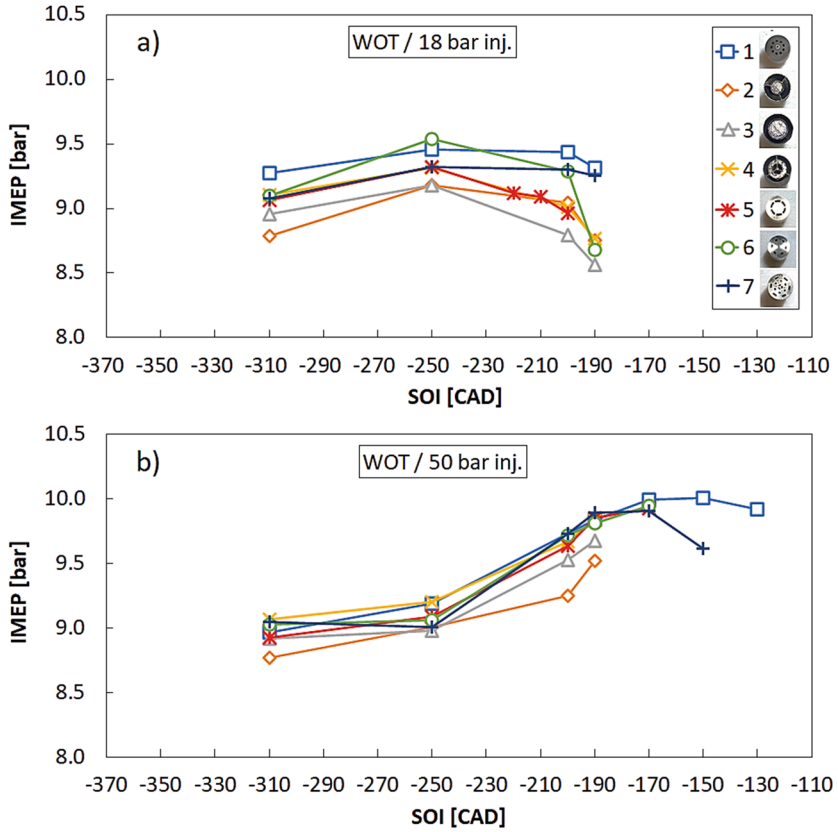

Fig. 5. Dependence of maximum IMEP for different injector nozzle heads at different SOI timings and injection pressures at 2000 rpm and WOT.

lowest CoV_{IMEP} values were achieved with nozzle heads 1, 6 and 7.

Different CoV_{IMEP} results for different injector nozzle heads were observed at WOT when the injection pressure was increased to 50 bar (Fig. 6c). At early injection timing (310 CAD bTDC), CoV_{IMEP} for most of the nozzle heads was in the range of ~1–2%. When a later SOI timing was applied (190–250 CAD bTDC), the combustion stability improved and CoV_{IMEP} was in the range of 0.5–1%. Some of the nozzles, e.g., nozzle heads 1 and 7, reached very late injection timing (130–150 CAD bTDC) together with low variation in IMEP. However, increasing the injection pressure to 50 bar did not improve the combustion stability for nozzle heads 2 and 3.

Overall, under both part load and WOT conditions and at early injection timings (250–310 CAD bTDC), the combustion stability was high. The largest differences were at late SOI and injection pressures requiring air/fuel mixing improvement.

Fig. 7 shows a comparison of the combustion duration CA10-90 for different nozzle types at part load (18 bar injection pressure) and WOT (18 and 50 bar injection pressure). At part load and 18 bar injection pressure, the combustion duration of all the nozzles remained the same until SOI reached 190 CAD bTDC (Fig. 7a), whereupon the combustion duration became shorter. This trend was especially evident with nozzle heads 1, 6 and 7. When the SOI timing reached 170 CAD bTDC, the combustion duration was more prolonged with most of the nozzles, in agreement with the decreased combustion stability findings (Fig. 7a). However, nozzle heads 1, 6 and 7 still showed the shortest combustion durations. Sevik et al. also showed that the flame development angle and combustion duration tended to be shorter at later SOI timings [50].

At WOT and 18 bar injection pressure (Fig. 7b), all nozzle heads showed a similar trend of CA10-90 when SOI was in the range 250–310 CAD bTDC. When the SOI timing was retarded further (up to 200 CAD bTDC), CA10-90 for some of the nozzle types (2, 3, 4 and 5) became longer than for others (1, 6 and 7). However, CA10-90 also started to increase for nozzles 1, 6 and 7 when SOI was later than 200 CAD bTDC.

Increasing the injection pressure to 50 bar under WOT conditions (Fig. 7b) resulted in different CA10-90 trends when the fuel was injected at the end of the intake stroke and during the compression stroke. The results for all nozzle types revealed that the combustion duration became shorter at 170–190 CAD bTDC timing than at 310 CAD bTDC. Nozzle head 1 achieved an even shorter combustion duration at 150 CAD bTDC. One of the main explanations of the improved combustion at WOT, late injection timing and high injection pressure is the combustion speed was improved by increased turbulence in the cylinder due to the high fuel injection pressure. This finding was also discussed by [14], who stated that late injection can considerably improve the turbulence and achieve faster combustion. The ability of DI-CNG to increase turbulence in the cylinder and improve combustion and the rate of heat release was also discussed in our previous study [42].

A comparison of the indicated specific fuel consumption (iSFC) is presented in Fig. 8. The error bars are not included because the variations in iSFC were very low between the samples. The results showed that there was no major difference between the nozzle heads when the fuel was injected during the intake stroke between 310 and 250 CAD bTDC either under part load (Fig. 8a) or WOT conditions (at both 18 and 50 bar injection pressures) (Fig. 8b and c). The only difference was observed at late injection (later than 190 CAD bTDC). The value of iSFC increased when the fuel was injected late for both 6 bar IMEP and WOT conditions (at 18 bar injection pressure). However, the 50 bar injection pressure cases at WOT showed that iSFC remained at the same level for all nozzle types. The same trend of better results in iSFC was found for nozzle heads 1, 6 and 7. The iSFC results clearly showed that different nozzles can influence ICE fuel consumption.

Among the tested nozzle head designs (Fig. 2), improved combustion was achieved with nozzle heads 1, 5, 6 and 7. These nozzle heads had multiple small holes, which could divide and spray smaller jets in the cylinder. In contrast, the injector nozzle heads 2, 3 and 4 tended to spray the fuel from larger holes and concentrated larger fuel amounts in

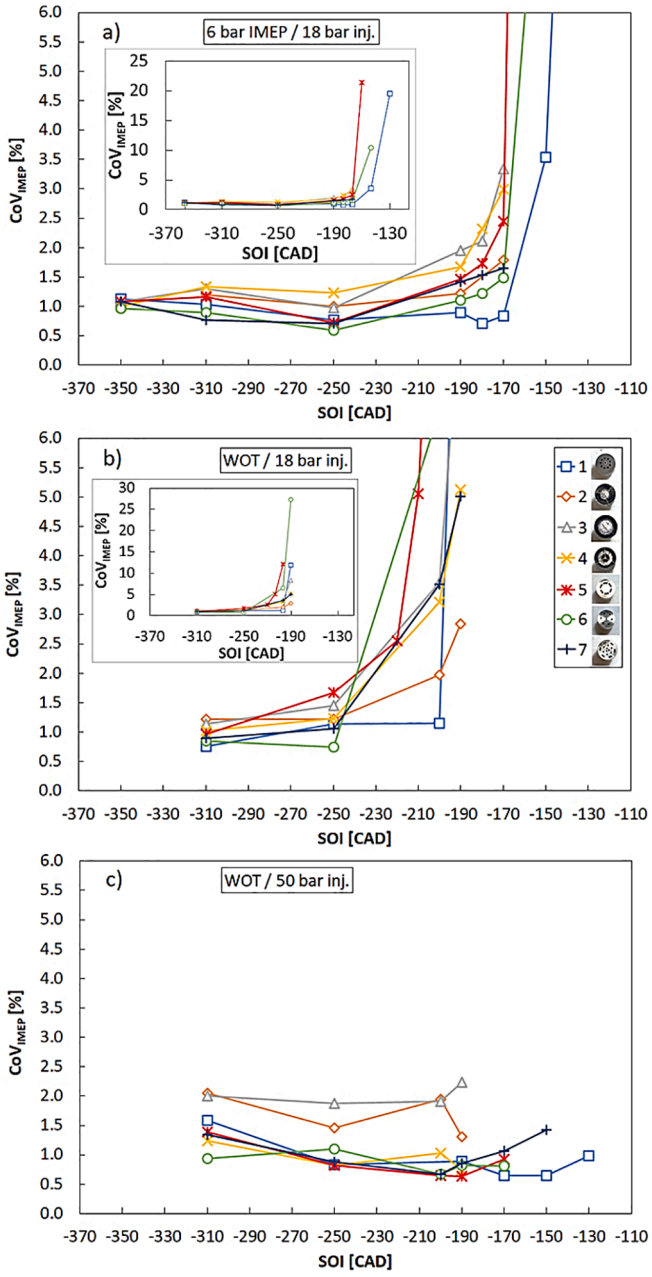

Fig. 6. Dependence of CoV_{IMEP} for different injector nozzle heads at different SOI timings, engine loads and injection pressures.

certain spray regions.

3.2. Standard emissions

Fig. 9 shows the $iSCO_2$ emissions for different nozzle heads at a part load of 6 bar IMEP and 18 bar injection pressure and WOT at 18 and 50 bar injection pressures.

At part load (Fig. 9a), $iSCO_2$ emission levels were ~480–520 g/kWh when SOI was changed from 350 to 190 CAD bTDC. Most of the nozzle heads showed the same level of CO_2 emissions with small increases at 250 CAD bTDC timing compared to 350 CAD bTDC. Similar findings were reported by [45], who showed that at early injection timings, CO_2 emissions increased due to improved air/fuel mixing. However, $iSCO_2$ emissions from the majority of nozzle head types started to decrease for SOI between 190 and 180–170 CAD bTDC. This trend agreed with the previously discussed increases in fuel consumption (Fig. 8a) and iSCO (Fig. 10) and iSHC emissions (Fig. 11). At a SOI timing later than 170 CAD bTDC, CO_2 emissions increased again for some of the nozzles. One explanation for this is the air/fuel mixing improved when the piston started moving up in the compression stroke and the turbulence increased due to piston movement. However, much later SOI (e.g. nozzle head 1 at SOI 130 CAD bTDC) showed a reduction in $iSCO_2$ emissions. A similar trend was observed by [50], who showed that CO_2 increased at later injection timings but decreased at much later timing due to reduced combustion efficiency.

High load conditions at both high and low injection pressures (18 bar and 50 bar) (Fig. 9b and c) showed similar CO_2 emission levels for all nozzles when the SOI timing was varied between 310 and 250 CAD. The main difference was at 18 bar injection pressure and later injection. Nozzle heads 3, 4, 5 and 6 showed increased CO_2 emissions up to ~550 g/kWh, whereas the other nozzles showed similar $iSCO_2$ emissions at 480–500 g/kWh. Other researchers have reported higher CO_2 emissions at late SOI (120 CAD bTDC) compared to early (360 CAD bTDC) [17]. Increased $iSCO_2$ emissions for nozzle heads 3, 4, 5 and 6 correlated with the increased iSFC values at late SOI, indicating that with higher fuel consumption, more CO_2 was formed.

Analysis of the WOT load case and 50 bar injection pressure revealed a slightly different trend. Even at late SOI timings, $iSCO_2$ emissions remained at the same level for all injector nozzle head types. This suggests that a higher injection pressure improved $iSCO_2$ emission levels for injector nozzle types (e.g., nozzle heads 3, 4, 5, 6) compared to a lower injection pressure at WOT. In the case of nozzle head 1, CO_2 emissions remained at the same level even at much later injection timings, i.e., 130 CAD bTDC.

Fig. 10 presents the iSCO emissions for the tested nozzle heads at different SOI timings. At part load conditions (6 bar IMEP) (Fig. 10a) and early injection timings (350 CAD bTDC), iSCO emission levels reached 16–24 g/kWh depending on the nozzle head type. Use of a later injection timing reduced CO emission to 7–16 g/kWh level (except for nozzle head 2). The most promising iSCO results were achieved with nozzle head 1, which emitted the lowest iSCO emissions over the whole SOI timing range. When the fuel was injected later (250–190 CAD bTDC), iSCO emissions started to increase for all nozzle types. However, nozzle head 1 showed low iSCO emissions even at 170 CAD bTDC injection timing.

A similar CO "dipped" curve at medium timing was observed by [50], with CO increasing again at later injection timing. The decreasing iSCO trend may be because at earlier injection timing, there was sufficient oxygen amount to achieve more complete combustion and oxidize CO to CO_2 [45,51]. However, in the present study, the oxidation was probably incomplete, resulting in the iSCO increase at late injections for some of the nozzle heads. As the exhaust gases during the expansion stroke cooled down, the CO oxidation rates would decrease [51], decreasing CO_2 emissions (Fig. 9a).

At high engine load (WOT) and low injection pressure (18 bar) (Fig. 10b), the lowest iSCO emissions of 12–21 g/kWh for all nozzle types were obtained at an early injection timing. The lowest emission levels were achieved with nozzle heads 1, 5, 6 and 7. iSCO emissions started to increase for all nozzles when the SOI timing was 250 CAD bTDC and continued to increase up to an injection timing of 190 CAD bTDC, reaching iSCO emission levels of 30 to 35 g/kWh. At late SOI, the differences in CO emissions between the nozzles were smaller than at early SOI (310 CAD bTDC).

At high load and high injection pressure (50 bar) (Fig. 10c), the iSCO emissions at early SOI was not much affected and were similar to those measured at 18 bar injection pressure. The main benefit of increased injection pressure for most of the nozzles was seen at a late injection timing of 190 CAD bTDC, where iSCO levels decreased to 7–14 g/kWh at 50 bar compared to 30–35 g/kWh at 18 bar injection pressure. The lowest iSCO emissions were achieved with nozzle head 1, whereas nozzle head 2 showed the highest levels over almost the whole SOI timing range. The results also agreed with the $iSCO_2$ emission levels

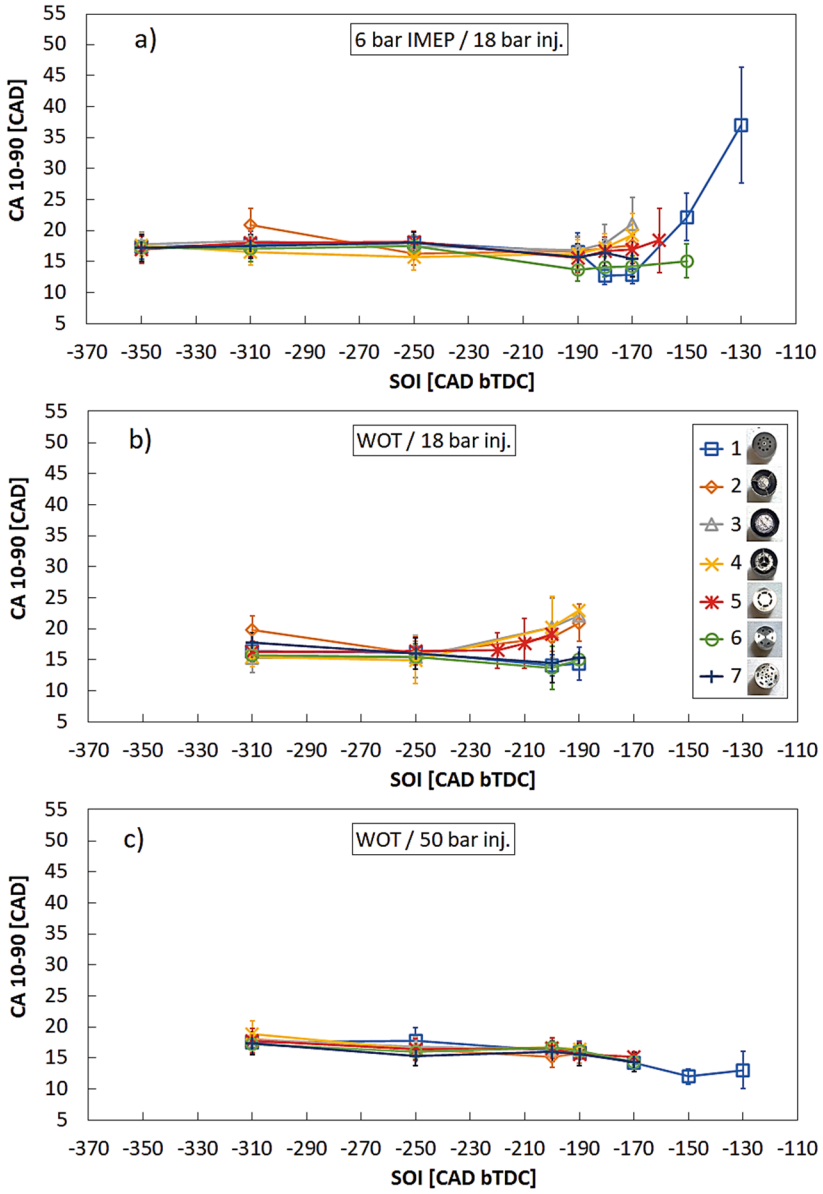

Fig. 7. Dependence of combustion duration (CA10-90) for different injector nozzle heads at different SOI timings, engine loads and injection pressures.

(Fig. 9c), i.e., CO_2 emission levels remained at similar levels with a slight increase at later injection timing, indicating that the oxidation of CO was improved at 50 bar compared to 18 bar injection pressure. Similar benefits of using a higher injection pressure at late injection timing were observed by [34]. One explanation for the improved iSCO emissions at 50 bar injection pressure is higher injection pressures increase the turbulence in the cylinder, which improves the combustion process and CO oxidation. Other researchers have also reported lower CO emissions at late injection timing and higher engine speed [17].

Fig. 11 shows the indicated specific hydrocarbon iSHC emissions for the different types of nozzles at different injection timings, loads and pressures. The parameter iSHC represents THCs, meaning that methane and nonmethane HC emissions are presented as a total value.

At part load and early SOI timing (350 CAD bTDC) (Fig. 11a), iSHC emissions were similar for all DI-CNG injector nozzle heads, reaching ~2 g/kWh. iSHC emissions started to slightly increase when SOI reached 250 CAD bTDC. However, the differences in emission levels between nozzle heads were only minor. Comparison between iSCO (Fig. 9a) and iSHC emissions at 350–250 CAD bTDC SOI timing demonstrated that at early injection timing, the combustion efficiency was higher and more complete combustion was achieved. On the other hand, CO emissions were increased due to decreased oxidation processes. At later injection timing, iSCO emissions decreased and iSHC started to increase, indicating that the combustion efficiency slightly decreased due to a lack of time for the air and fuel to mix fully just before the ignition. Other researchers have also observed increased THC emissions from DI-CNG at late injection timings, which were attributed to insufficient air/fuel mixing [45]. It has also been reported that at late SOI (between 210 and 150 CAD bTDC), increased HC emissions due to poor fuel mixing resulted in a slow combustion rate and increased combustion duration [52]. Similar findings were obtained by [53], who showed that a late injection timing caused mixture homogeneity issues, incomplete combustion process, higher CoV_{IMEP} and increased CO and HC emissions. They also reported that at high speed and medium loads, an early injection was essential to maximize the mixing time between the end of injection (EOI) and spark timing [53].

Further delaying the SOI timing (up to 190 CAD bTDC) revealed that iSHC emissions were higher (reaching 3.5 g/kWh) and the differences in HC emissions between the nozzle head types were increased compared to early injection timing points. At timings later than 190 CAD bTDC,

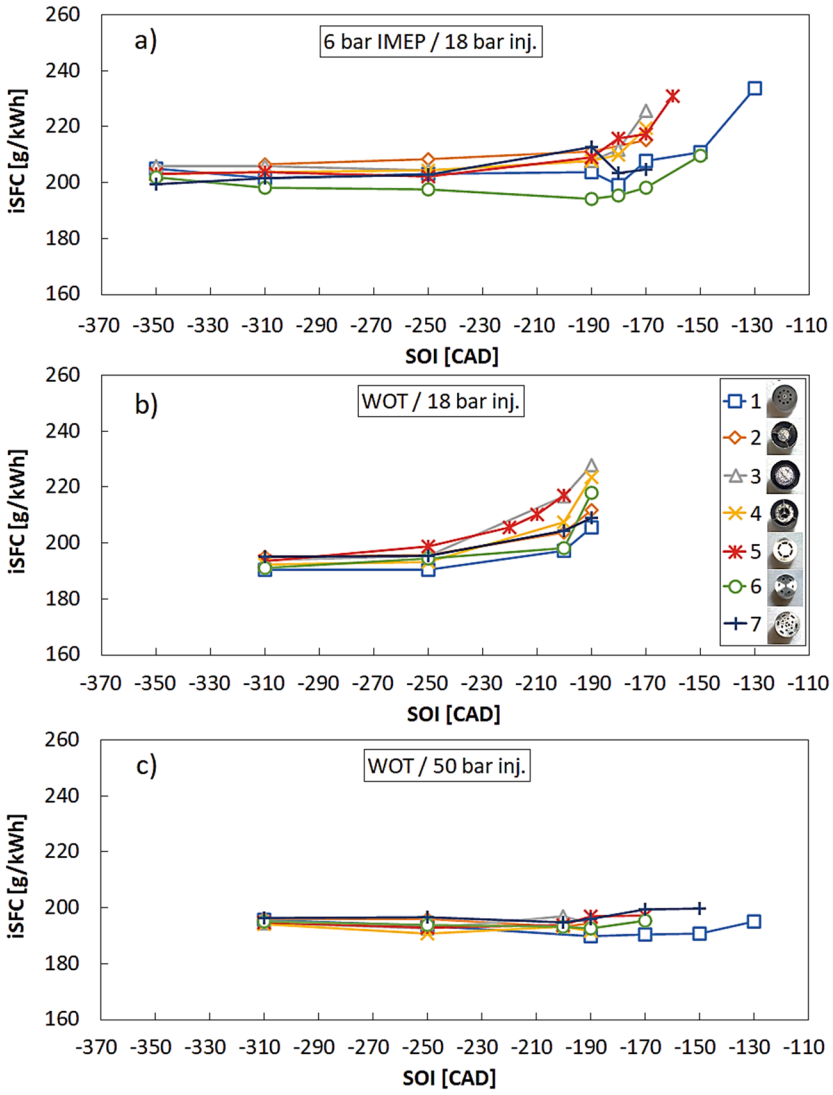

Fig. 8. Dependence of iSFC for different injector nozzle heads at different SOI timings, injection pressures and engine loads.

there was a sharp increase in iSHC. The earliest increase and highest value of iSHC (at 180–170 CAD bTDC) were obtained with nozzle heads 2, 3, 4 and 5. The lowest and the most promising results were achieved with nozzle head 1, which maintained low iSHC emission levels even at 150–170 CAD bTDC SOI.

At high load and low injection pressure (Fig. 11b), iSHC emissions from the majority of nozzle heads decreased when the SOI timing was changed from 310 to 200–210 CAD bTDC. The values were reduced from ~2.8–3.5 g/kWh to 1.5–2.5 g/kWh. A similar trend of decreased THC emissions with later injection was also demonstrated by [34]. Such a reduction in iSHC might be related to improved air/fuel mixing under WOT conditions, which would increase the combustion efficiency. However, nozzle heads 2 and 4 (with bigger dead volume inside the nozzle heads and having wider crevices) showed a different trend in iSHC emissions than the other nozzle types at timings later than 250 CAD bTDC. At SOI timings later than 200 CAD bTDC, iSHC emissions started to increase also for nozzle heads 1, 3, 5, 6 and 7.

At WOT and 50 bar injection pressure (Fig. 11c), iSHC emission levels were slightly improved at early SOI (310 CAD bTDC) compared to the 18 bar injection pressure cases. However, HC emissions showed a slightly different trend at the increased injection pressure. HC emissions from all tested nozzles increased when the injection timing was delayed at 50 bar injection pressure. Slight iSHC increase at higher injection pressures might be related to a formation of fuel rich zones and the presence of gaseous fuel in the cylinder crevices or interaction with cylinder liner, as discussed later. The lowest iSHC values were achieved with nozzle heads 1, 5, 6 and 7. Comparison between the 310 CAD bTDC injection point at 18 and 50 bar injection pressure showed that at the lower injection pressure, iSHC was slightly higher (2.8–3.2 g/kWh) compared to that at 50 bar pressure (2–3 g/kWh). The higher HC emissions at lower injection pressure might be related to air/fuel mixture inhomogeneity. Seboldt et al. reported that at higher injection pressures, HC emissions decreased due to increased jet penetration [49]. Tests showed that at higher injection pressures, stagnated axial penetration converts to radial penetration, resulting in a wider jet. The deeper and wider penetration improves air entrainment and mixture formation [49].

Although some researchers have reported that HC emissions are lower at early injection timing, several studies have demonstrated that very early or late injection can increase HC emissions due to the formation of fuel-rich mixture zones [17]. It has also been shown that HC emissions tend to increase with lower injection pressure at early SOI timing [34] (similar to the results obtained in the present study) due to the presence of unburned fuel in crevices and wall quenching. In addition, it has been reported that early injection timings may increase iSHC emissions due to increased fuel and cylinder liner contact [31]. Our

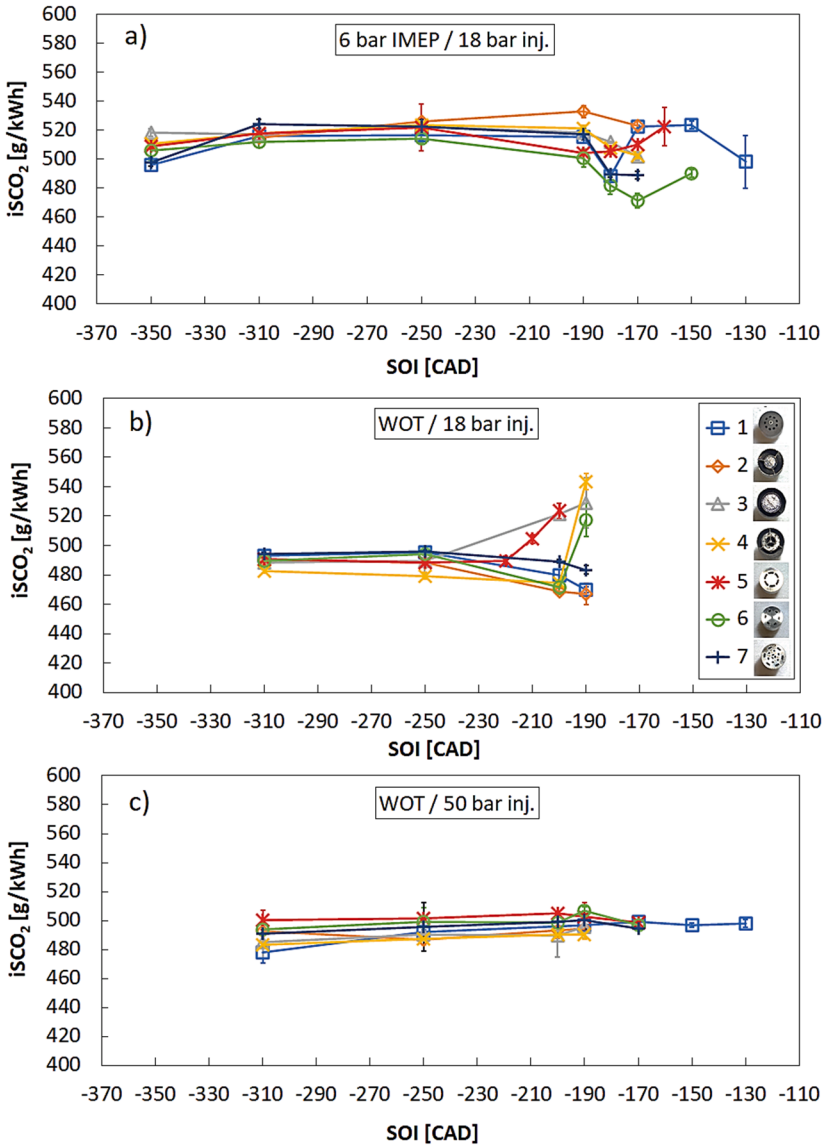

Fig. 9. Dependence of $iSCO_2$ emissions for different injector nozzle heads at different SOI timings, engine loads and injection pressures.

investigation of iSCO and iSHC emissions for different injector nozzle types showed that nozzle heads that injected the fuel more toward the central part of the cylinder (nozzle heads 1, 5, 6 and 7) achieved lower emissions for a broad range of SOI timing under both part load and high load conditions than nozzle heads that concentrated the fuel more toward the cylinder wall (nozzle heads 2, 3 and 4) with umbrella and swirl type injection. A similar trend has been observed by other researchers, who showed that a toroidal vortex type jet (with a smaller hollow cone nozzle angle) can reduce the crevice flow and unburned HC emissions [31]. It was also stated that with early injection timing, fuel and liner interaction cannot be avoided [31]. In the present study, it was also clear that nozzles with a tendency to form a mixture more toward the cylinder liner (nozzle heads 2, 3 and 4) showed higher iSHC emissions than nozzles forming a mixture concentrated in the central cylinder part.

Comparison of the low and high load results at two different injection pressures (Fig. 11b and c) showed that differences between iSHC emissions were small for SOI timing between 310 and 190 CAD bTDC. Other experimental DI-CNG studies have shown a similar trend, with the injection pressure having only a minor influence on HC formation [49]. Such findings suggest that lower injection pressure is preferable owing to the possible drivable mileage dependency on the lowest possible fuel pressure in the fuel tank if earlier injection timings are applied [49].

Fig. 12 presents the indicated specific NO_x emissions ($iSNO_x$) for the different nozzle heads at 6 bar IMEP and WOT and at different injection pressures and SOI timings.

Results of the part load tests (Fig. 12a) showed that $iSNO_x$ increased from 6.3 to 7.5 g/kWh at 350 CAD bTDC timing to 7.5–8.5 g/kWh at 310 CAD bTDC with only slight differences in $iSNO_x$ values between the different nozzles. When the injection timing was delayed to 250 CAD bTDC and later, the differences in $iSNO_x$ values increased between the nozzles, e.g., varying from 5.5 to 8 g/kWh at 190 CAD bTDC. In addition, $iSNO_x$ emissions showed a decreasing trend with later SOI timings. The highest $iSNO_x$ levels were achieved with nozzle head 1 over a broad range of SOI timing. This finding was supported by the CA10-90 plot (Fig. 7a). The combustion duration for nozzle head 1 was shorter than the other nozzle types, meaning that the heat released from the fuel was more intense over a shorter period of time, resulting in an increased combustion temperature and increased NO_x formation.

Tests at increased engine load (WOT) and 18 bar injection pressure (Fig. 12c) revealed a similar trend as for the part load conditions. $iSNO_x$ was highest at early injection timing, e.g., $iSNO_x$ decreased from 9.5 to 10.8 g/kWh at 310 CAD bTDC to 4.5–6 g/kWh at 190 CAD bTDC.

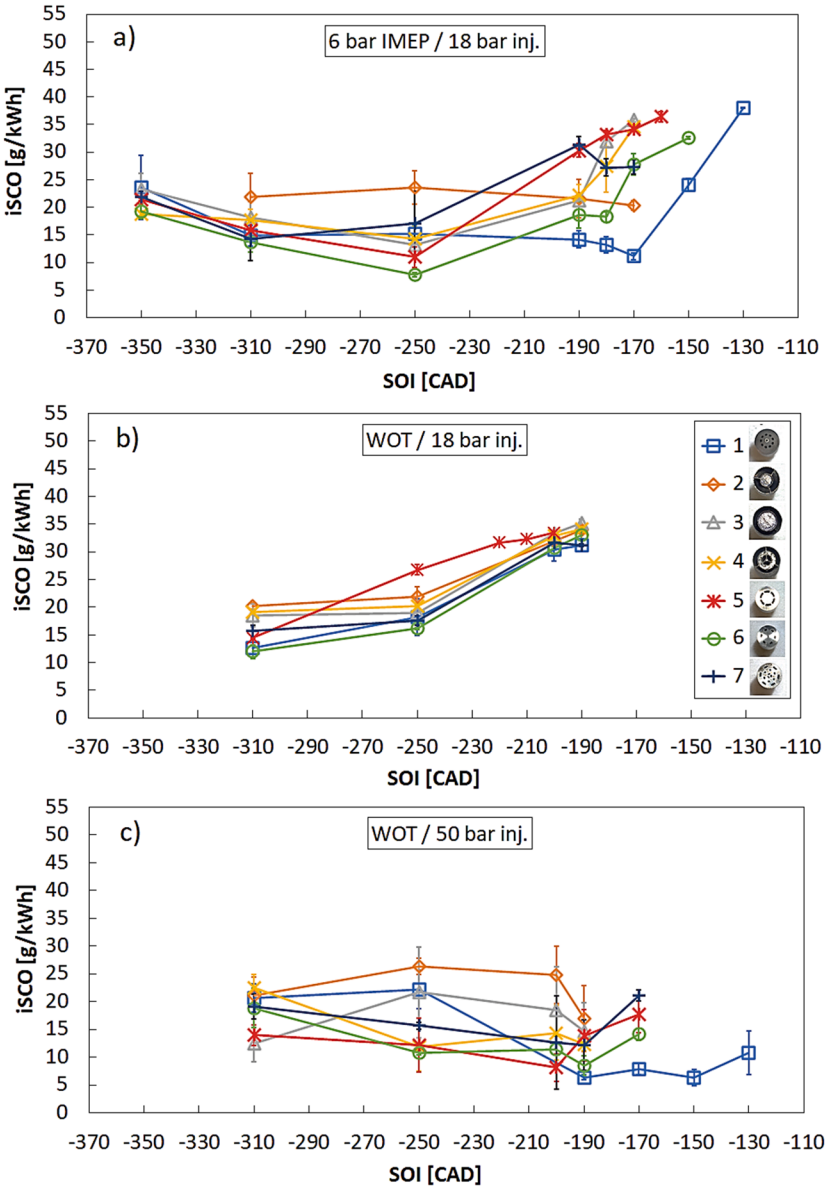

Fig. 10. Dependence of iSCO emissions for different injector nozzle heads at different SOI timings, engine loads and injection pressures.

These findings agree with other studies showing NO_x is reduced at later injection timings [17]. The reduction in $iSNO_x$ emissions is likely due to slower combustion and a reduced exhaust temperature [52]. Slower combustion may be a consequence of reduced turbulence in the cylinder when the piston slows down at the end of the intake stroke and air/fuel mixing is reduced. This explanation is supported by the test results from the same engine load point but with 50 bar injection pressure applied (Fig. 12c).

The trends in $iSNO_x$ emissions at 50 bar injection pressure at later injection timings were different than for the 18 bar injection pressure cases. At WOT and 50 bar injection pressure, all the injector nozzle heads showed increased $iSNO_x$ emissions. A higher injection pressure improves turbulence in the cylinder, which increases the combustion temperature and results in higher NO_x level formation. This finding was supported by the iSCO results (Fig. 10). Increased turbulence and higher combustion temperature increase the oxidation of CO emissions, as shown by the decreasing trend in iSCO with increasing injection pressure. Higher injection pressure also improves mixture homogeneity. Also, the emission trends of $iSNO_x$ and $iSCO_2$ showed increasing trends at later SOI timings (190–250 CAD bTDC) while at the same time iSCO showed a reduction with most of the nozzles (except nozzles 2 and 3) which means that combustion temperature and oxidation process were higher. Again, this proves that the combustion process can be improved not only with a combination of higher injection pressure, late injection timing but also with a specifically designed injector nozzle head. Other studies also have shown that at later SOI timings, NO_x emissions were lower at lower injection pressure than at higher injection pressure [34].

3.3. Total PN and images of the combustion process

The analysis of standard emissions showed that SOI timing and nozzle type can influence emission levels. Further investigation focused on PN emissions. As mentioned above, there is still a lack of information about PN emissions from DI-CNG systems when different SOI timings are applied, and especially when different nozzle head designs are used for the gas jet formation.

Fig. 13 shows the total PN results for different nozzle heads under the tested conditions. At part load (6 bar IMEP) (Fig. 13a), total PN for all nozzle head types was in the range ~20×10^5-$3x10^6$ #/cm^3 when the SOI timing was 310–350 CAD bTDC. A similar total PN level was

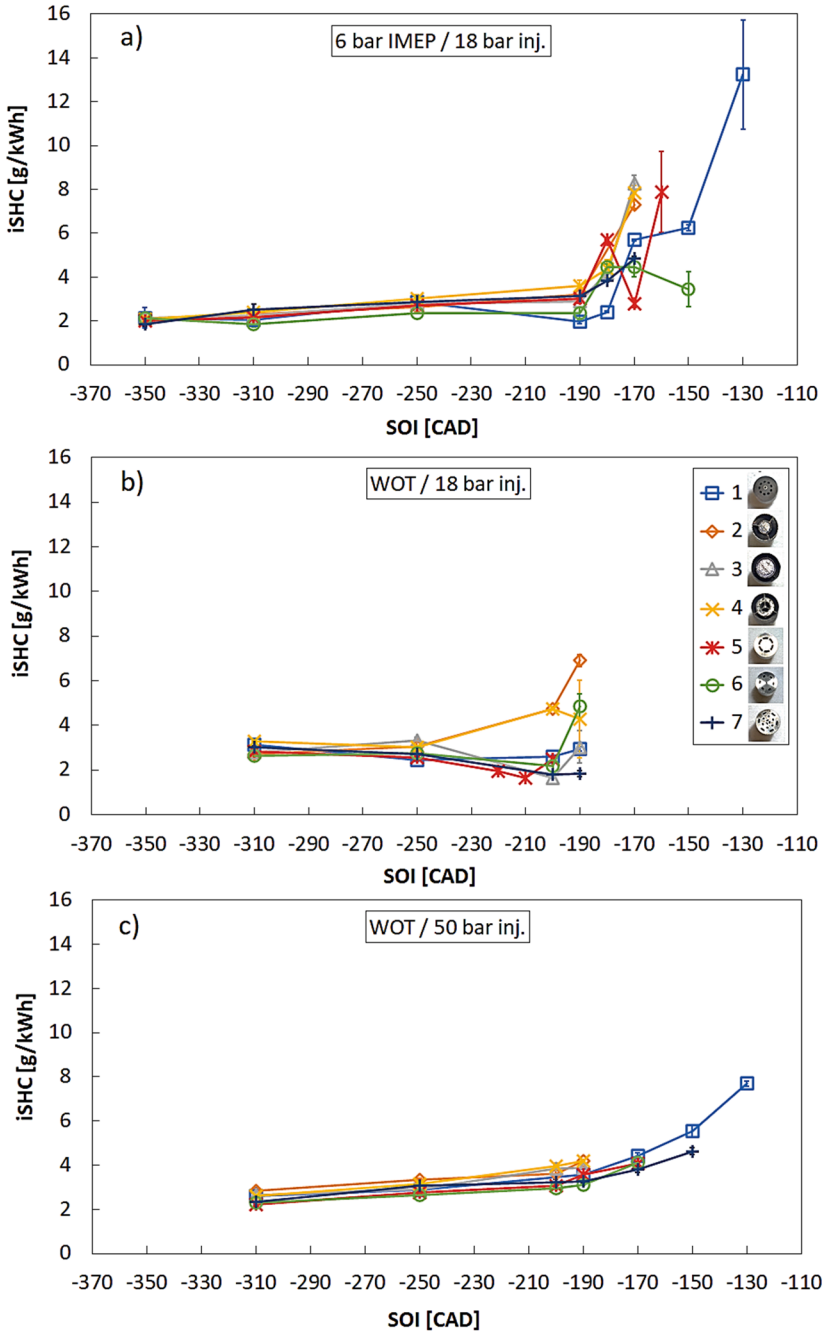

Fig. 11. Dependence of iSHC emissions for different injector nozzle heads at different SOI timings, engine loads and injection pressures.

observed for nozzle heads 1, 5, 6 and 7 when the injection took place at the end of intake stroke or at the beginning of the compression stroke (170–250 CAD bTDC). However, nozzles 2, 3 and 4 showed an increasing trend for PN emissions for the same SOI timing range, with PN emissions reaching $2x10^7$-$1x10^8$ #/cm^3. However, at later injection timing (130–170 CAD bTDC), PN emissions also started to increase for the other nozzle types.

WOT tests at 18 bar injection pressure (Fig. 13b) showed that total PN emissions from different nozzle heads at early injection timing were at a similar level to those measured under part load conditions. In addition, there was a similar early increase of PN for nozzle heads 2, 3 and 4 when the fuel was injected at 250 CAD bTDC and later. However, PN started to increase for the other nozzle types when SOI reached 200–220 CAD bTDC. Nozzle head 1 achieved the lowest PN (~$7x10^7$ #/cm^3) at late SOI timing (190 CAD bTDC). However, most of the nozzle types reached much higher total PN ($7x10^8$-$3x10^9$ #/cm^3) at late 190 CAD bTDC timing.

Seboldt et al. showed that PN emissions were relatively low for a range of SOI timings from early to late and either with low (20 bar), either with high (110 bar) injection pressures [38]. However, the trends in PN were different from the present findings. One reason for this is the present study involved high load points, whereas Seboldt et al. tested at lower load conditions. Also, the PN measurement technique was different from the present investigation. Other research also showed that CNG can generate PN emissions at levels of $1x10^7$ #/cm^3 and the measurement did not include any volatile removing technique. It was concluded that the main contribution to PN emissions was burnt lubrication oil (PFI-CNG system) [54]. However, Adlercreutz et al. stated that CNG combustion may generate 1 to 5 nm particles [55]. It was determined that at higher engine loads and speeds CNG combustion can give

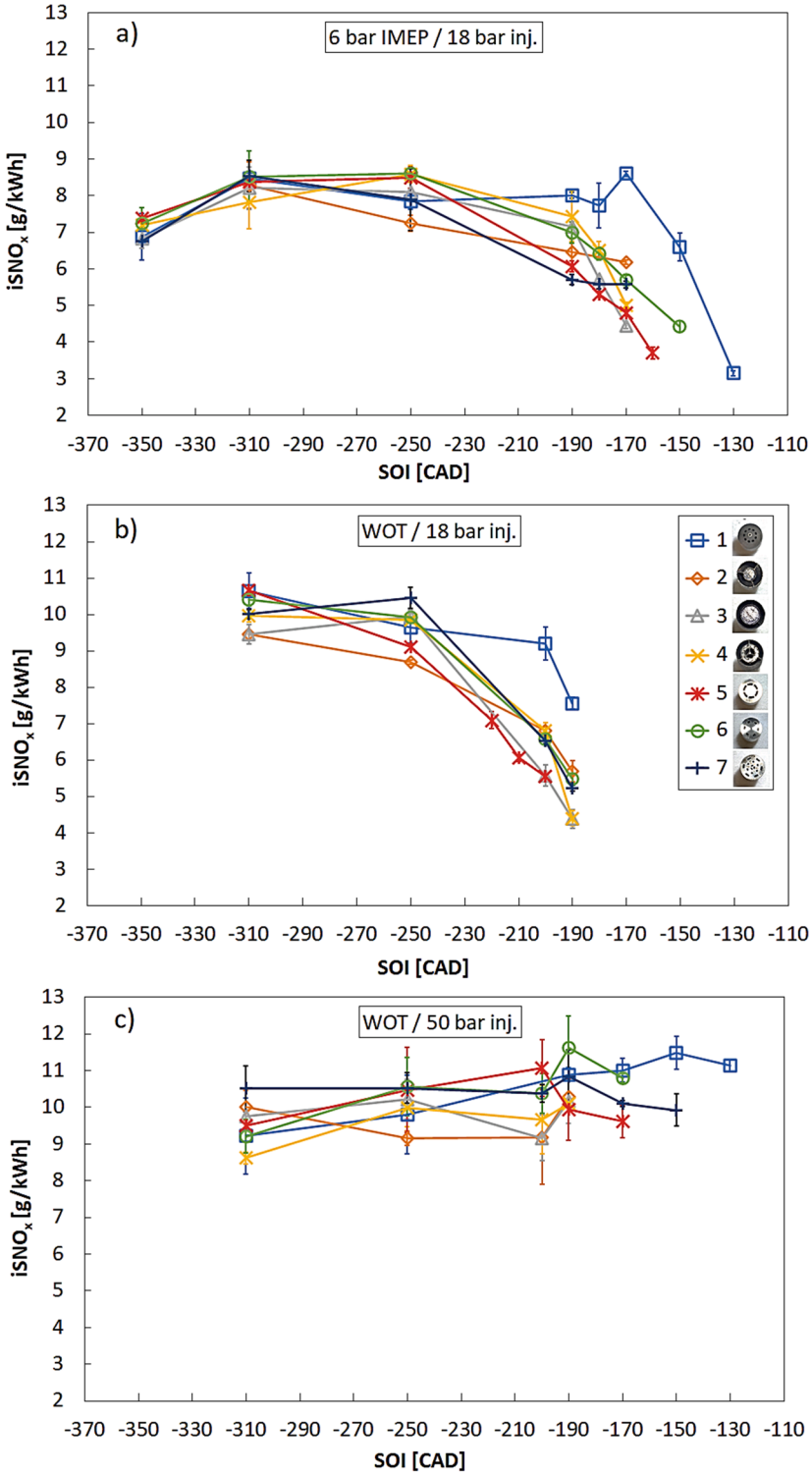

Fig. 12. Dependence of $iSNO_x$ emissions for different injector nozzle heads at different SOI timings, engine loads and injection pressures.

larger (accumulation mode) particles which resulted also in higher total PN [56]. In the present study, several mechanisms influence soot formation from methane fuel. These mechanisms give different soot and total PN formation levels. One of the soot formation mechanisms can be attributed to early injection timings from 250 to 310–350 CAD bTDC. At these injection timings, there is relatively enough time to mix fuel with air and reach high stoichiometry. Injector nozzle head design plays a small role in soot formation at early injection timing because injected gaseous fuel has enough time to mix with the air in the cylinder. However, given results show that injector nozzle head design has more influence on total PN emissions at later injection timing, and especially at higher engine loads (Fig. 13b) with lower injection pressure. The total PN increased to higher levels for all nozzles head types at late injection timing (190 CAD bTDC and later) meaning that another soot formation mechanism appears which is related to a shorter air/fuel mixing time, formation of fuel rich zones. Also, it can be related to the fuel injection pattern due to the injector nozzle head design which can lead to a diffusion fire or pool fires [57]. Increased soot formation and higher PN

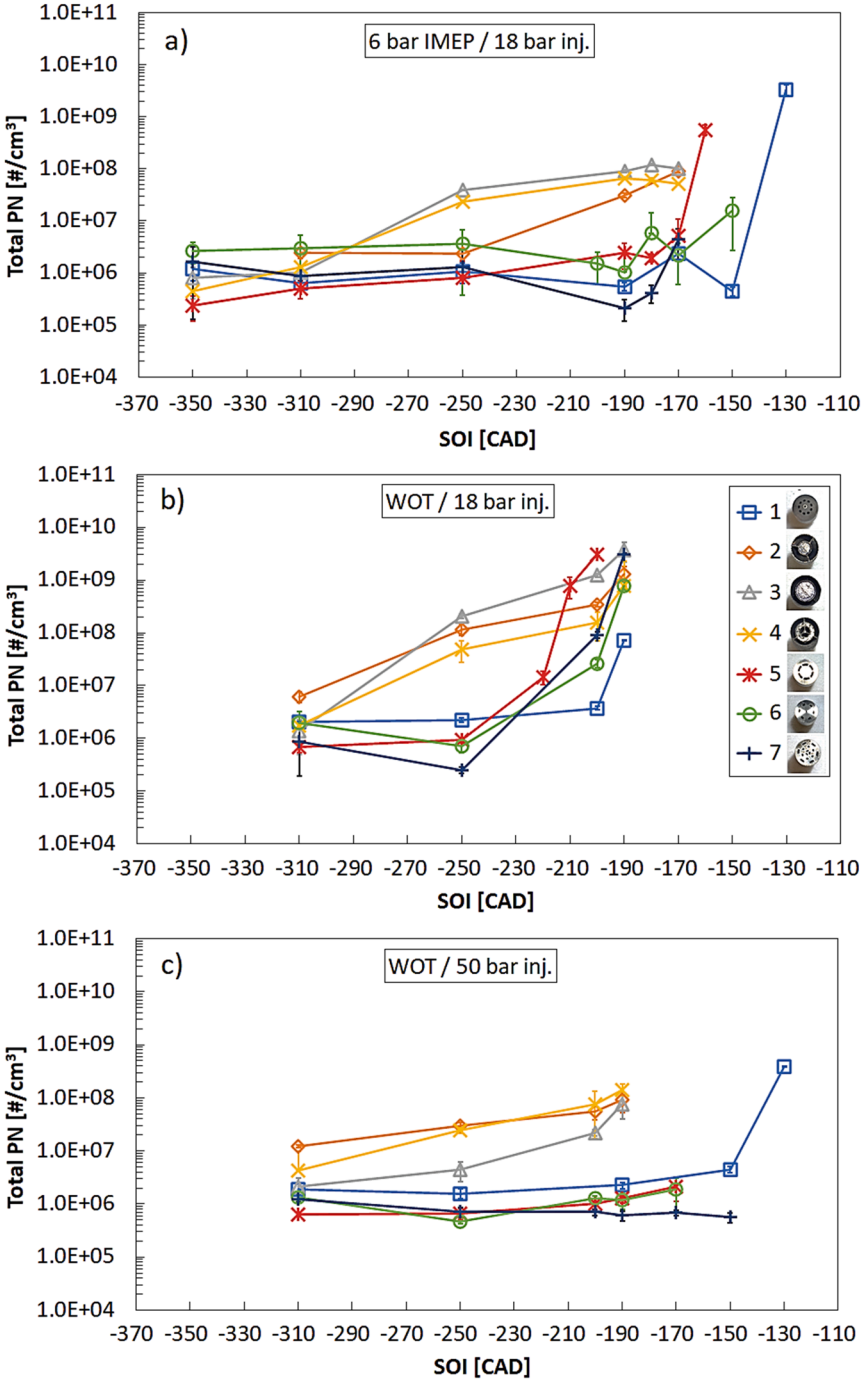

Fig. 13. Dependence of total PN emissions for different injector nozzle heads at different SOI timings, engine loads and injection pressures.

levels at late injection timing with all nozzle head designs also can be tracked for lower engine load 6 bar IMEP case (Fig. 13a). It should be noted that soot formation also depends on injected fuel mass. Thus, the higher fuel consumption could have led to higher PN formation. Indicated specific fuel consumption increased for all nozzle types at lower injection pressures (18 bar) and at late injection timings when the engine was tested at 6 bar IMEP and WOT conditions (Fig. 8a and b). Increasing iSFC trend also correlated with previously presented total PN trends (Fig. 13a and b). What is more, the total PN trends correlated with iSHC emissions trends either for lower engine load (6 bar IMEP), either for WOT conditions (Fig. 11a–c) at later injection timings. This means that combustion efficiency was lower, fuel rich zones were formed which led to increased hydrocarbon emissions and higher PN levels.

Measurements of WOT conditions and increased injection pressure of 50 bar (Fig. 13c) showed that total PN for nozzle heads 1, 5, 6 and 7 remained at low levels even at very late injection timings (150–190 CAD bTDC). For example, PN started to show a sharp rise for nozzle head 1 only at 130 CAD bTDC. However, some of the nozzle heads (2, 3 and 4) did not show a reduction in particulate formation even at high fuel injection pressure. At late SOI timing (190 CAD bTDC), PN was increased compared to early timing (310 CAD bTDC). Total PN levels for nozzle heads 1, 5, 6 and 7 were in the range ~4×10^5–2×10^6 #/cm^3 between 310 and 190 CAD bTDC timing, whereas for nozzle heads 2, 3 and 4, total PN was ~3×10^6–1×10^8 #/cm^3.

Further investigation of DI-CNG injector nozzle heads involved combustion image analysis from different load points, injection timings

and injection pressures. Combustion images helped to understand and give additional explanations for the combustion process, soot formation and support total PN results. Fig. 14 presents the combustion process for different injector nozzle heads at part load and 18 bar injection pressure when the fuel was injected at 310 CAD bTDC and 190 CAD bTDC. These injection timings were chosen to compare with the previously presented data. The images are presented for a single combustion cycle for each nozzle type.

Images from the early injection timing at part load and 18 bar injection pressure showed (Fig. 14a) that the combustion process was similar for most of the nozzle heads after the spark timing. All nozzle heads showed mainly blue flame development with no presence of yellow flame formation. The combustion images for nozzle heads 1, 5, 6 and 7 showed that at 6 bar IMEP and 190 CAD bTDC injection timing, only a blue flame was formed. Comparison of the images at 310 and 190 CAD bTDC injection timing showed that the flame development was faster and reached the visible endoscope boundaries earlier with the late injection timing. This demonstrates that the combustion process could be improved by using a later SOI timing.

Slightly different blue flame development phenomena were observed with nozzle head 2, i.e., swirl type nozzle head. The blue flame development from this nozzle type was slower than for the other nozzle heads. Images recorded at late SOI (190 CAD bTDC) (Fig. 14b) revealed that nozzle heads 2, 3 and 4 showed yellow flame formation late in the combustion process (~40–60 CAD after the spark). It can be seen from the combustion images that during the initial flame development stage, a blue flame was formed. Later, a yellow flame started to appear in the vicinity of the spark plug and injector. Other research groups [58] also detected a yellow-white flame during a DI-CNG combustion test. The flame was surrounded by a light blue flame. It is known that yellow flame formation is related to worse air/fuel mixing, more fuel-rich areas and soot formation. Bartolucci et al. also reported that the formation of a fuel-rich region in the vicinity of the spark plug electrode resulted in increased HCs as there was not sufficient oxygen to oxidize the fuel [51].

The combustion images support the PN measurement results under the same testing conditions (Fig. 13a), which showed that total PN levels were increased for nozzle heads 2, 3 and 4 due to yellow flame appearance at later combustion phase compared to the other injector nozzle head types.

Different research groups have tried to explain the particulates and soot formation either for liquid, either for gaseous fuels. Certainly, DI technology with liquid fuel (gasoline, ethanol) produces much more

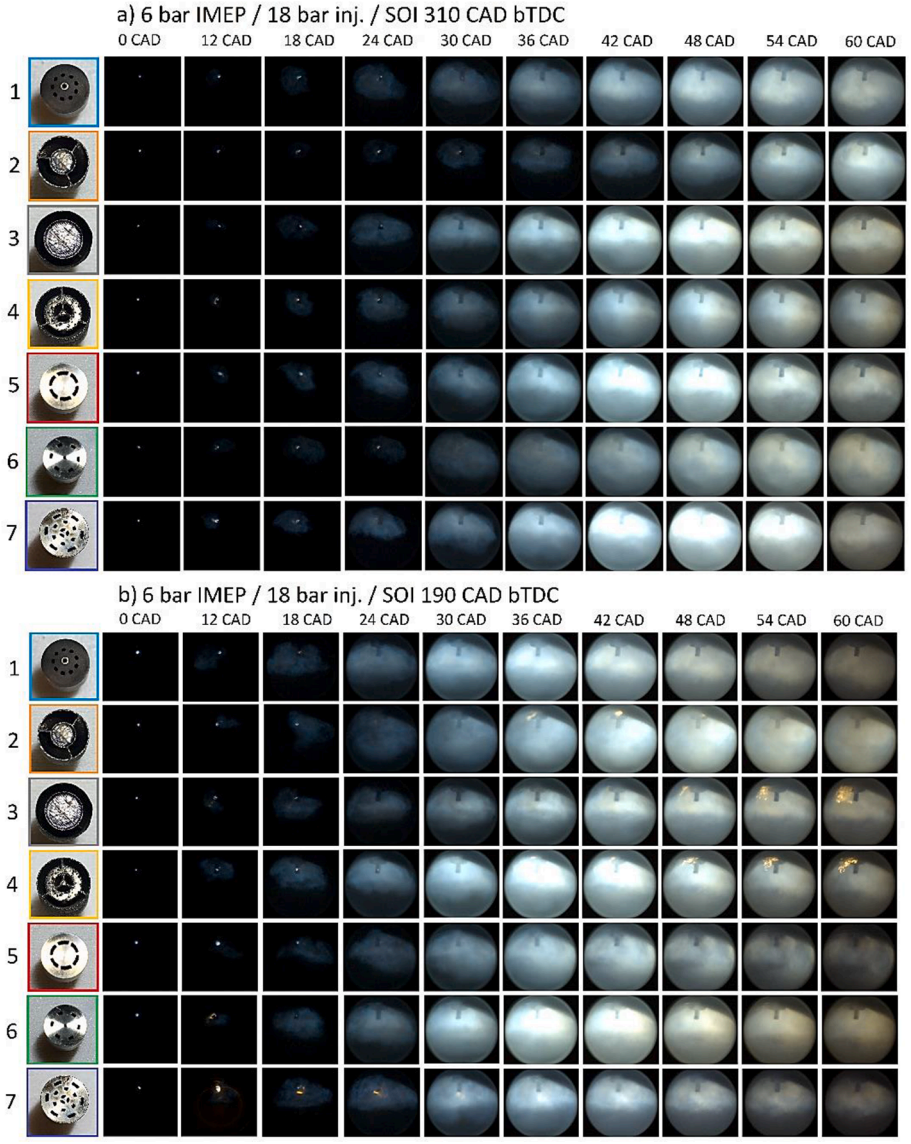

Fig. 14. Combustion process images for different injector nozzle heads at 310 CAD bTDC and 190 CAD bTDC injection timing. Part load conditions, 18 bar injection pressure.

particulates than gaseous fuel – methane (also methane-based fuels – natural gas and biogas). It was explained that soot formation from liquid fuels (GDI) can depend on several factors – the local stoichiometry temperature, pressure, and air/fuel mixing [59]. Locally fuel-rich zones in the cylinder are created due to bad mixing conditions. In the absence of oxygen and at a certain temperature fuel molecules are decomposed into active radicals H, OH, CH_3 and small molecule species such as ethylene (C_2H_4) and acetylene (C_2H_2). Mentioned radicals and species form polycyclic aromatic hydrocarbon (PAH) molecules which are precursors to form soot particles [60]. Soot emissions in engines depend on the competition between two processes – soot formation and soot oxidation. Combustion temperature in the cylinder can vary depending on operating conditions (e.g. low or high engine load, low or high engine speed) and injection parameters (e.g. injection timing, injection pressure). The temperatures can reach ~2400 K at which soot can be rapidly burned. Also, the temperature can fall to ~1500 K in regions where pool fires form during late stages of combustion, which may be too low for soot oxidation [57,59]. This was also proven with alternative fuel – methanol where maximum soot values were achieved at ~1600–1700 K temperatures and at later combustion phases [61]. Considering methane gas, it does not have carbon-to-carbon molecular bonds. Also, it has a simpler molecular structure which gives fewer chances to form benzene rings and leads to lower soot formation [62]. However, studies on methane pyrolysis at high-temperature mechanisms showed that ethane, ethylene and acetylene are also forming as for liquid fuels [63,64]. And it is known that two competing processes occur in sooting flames – firstly the soot precursors formation via acetylene pyrolysis and the second one – the oxidative degradation of these precursors by OH radicals [59,65]. High temperatures increase the rates of both processes, but the rate of oxidation increases more rapidly [63]. The higher the temperature, the lower the tendency of premixed flames to soot. Diffusion flames have different mechanisms because there is no oxidative attack on soot precursors in these flames. However, the pyrolysis rate still increases with temperature, leading to a higher rate of soot formation. The tendency to soot is greater when the flame temperature is lower [66]. Mentioned description of soot formation supports the present study findings that at late injection duration there is a lack of time to mix air and fuel for specific nozzle heads. Also, the combustion temperature was lower because $iSNO_x$ results (Fig. 12a) showed a decreasing trend at late SOI timings. Fuel-rich zones were formed which resulted in low intensity diffusion burn or pool fires at the nozzle tip or at spark plug crevices when the combustion process developed ~36 or

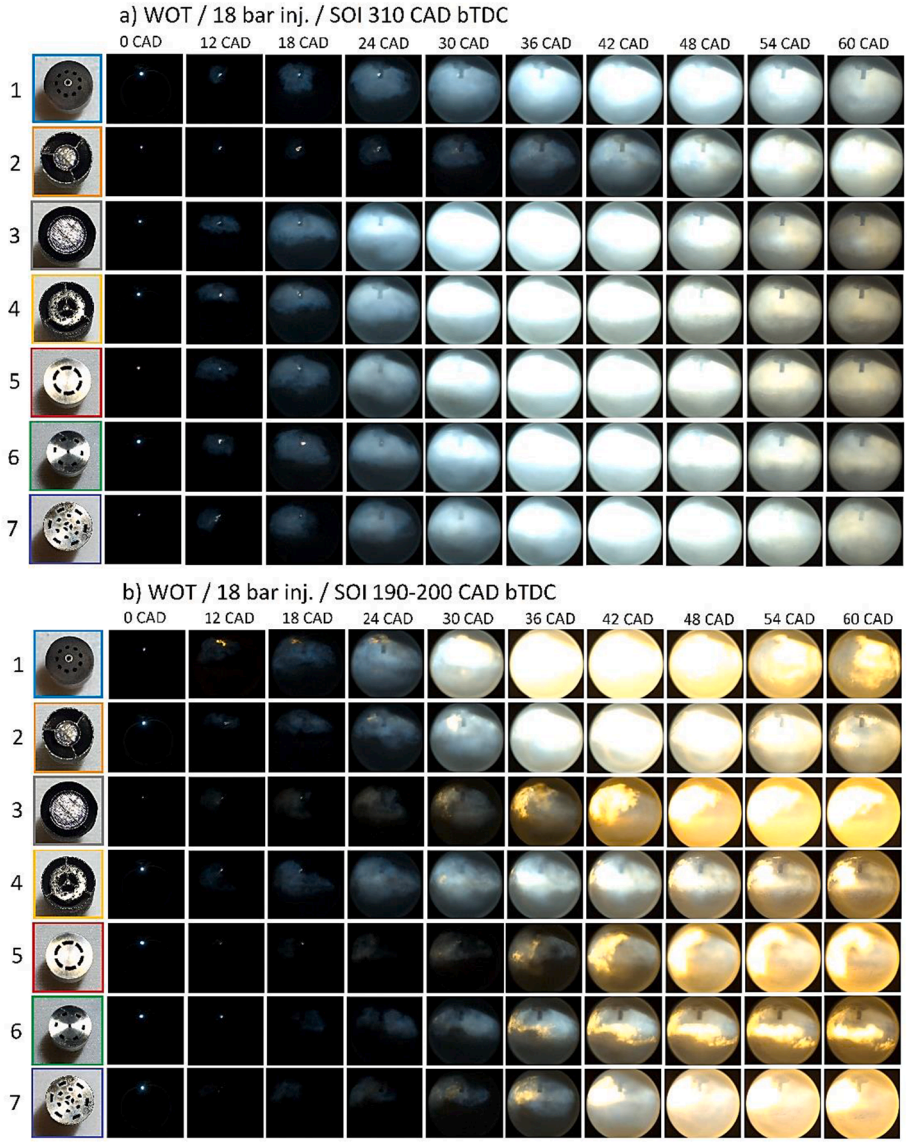

Fig. 15. Combustion process images for different injector nozzle heads at 310 CAD bTDC and 190–200 CAD bTDC injection timing. WOT conditions, 18 bar injection pressure.

~48 CAD (depending on nozzle head design) after the spark ignition. The rate of soot oxidation was reduced by the lower amount of OH radicals in the rich air/fuel regions. It is known that OH radicals are dominant oxidants that oxidize carbon. After that carbon is not involved in a soot particle formation [67,68]. This proves that the reduced soot oxidation process at the later combustion phase increased total PN levels for nozzle heads 2, 3 and 4 (Fig. 13b).

Fig. 15 shows images of the combustion process for different nozzle heads at WOT conditions and 18 bar injection pressure when the fuel was injected at 310 and 190 CAD bTDC.

The combustion images from the early injection timing (Fig. 15a) showed a similar trend to that observed at part load. The early injection timing did not show any fuel-rich zone formation (source of yellow flame) and only a blue flame was present. Similarly, to the part load case, nozzle head 2 showed different combustion behavior than the other nozzles. The flame developed more slowly and later for nozzle head 2 compared to the other nozzle types.

Analysis of the combustion process at late injection timing 190–200 CAD bTDC (Fig. 15b) revealed that the use of a low 18 bar injection pressure could cause issues related to air/fuel mixing. The combustion of all nozzle head types showed that a yellow flame (diffusion burn or pool fires) was present, which appeared at relatively early timing after the spark, i.e., 24–30 CAD after the start of ignition. Images from all nozzle heads showed that the yellow flame formation was very dense and present until a very late combustion process stage. Since yellow flames are related to the fuel-rich zone formation, decreased air/fuel mixing, reduced soot oxidation and increased particulate formation, its presence supports the previous finding that PN emissions (Fig. 13b) increased because of worse air and methane fuel mixing at late injection timing.

Combustion images were also recorded at increased injection pressure (50 bar) and WOT for the different injector nozzle heads (Fig. 16). Images obtained at SOI timing of 310 CAD bTDC again showed that the air/fuel mixture was well mixed with just a blue flame present, as observed with the other tested condition at early injection timing (Fig. 16a). Images captured at late injection (Fig. 16b) showed that a higher injection pressure improved the air/fuel mixing process for all the injector nozzle types. Mainly just a blue flame appeared during the combustion, even when the fuel was injected at late timing. The combustion process was very different compared to that at 18 bar injection pressure, where the yellow flame formation was dominant for all nozzle types. Increasing the injection pressure enabled the fuel to be injected in a shorter time, allowing enough time to mix the air and fuel and forming

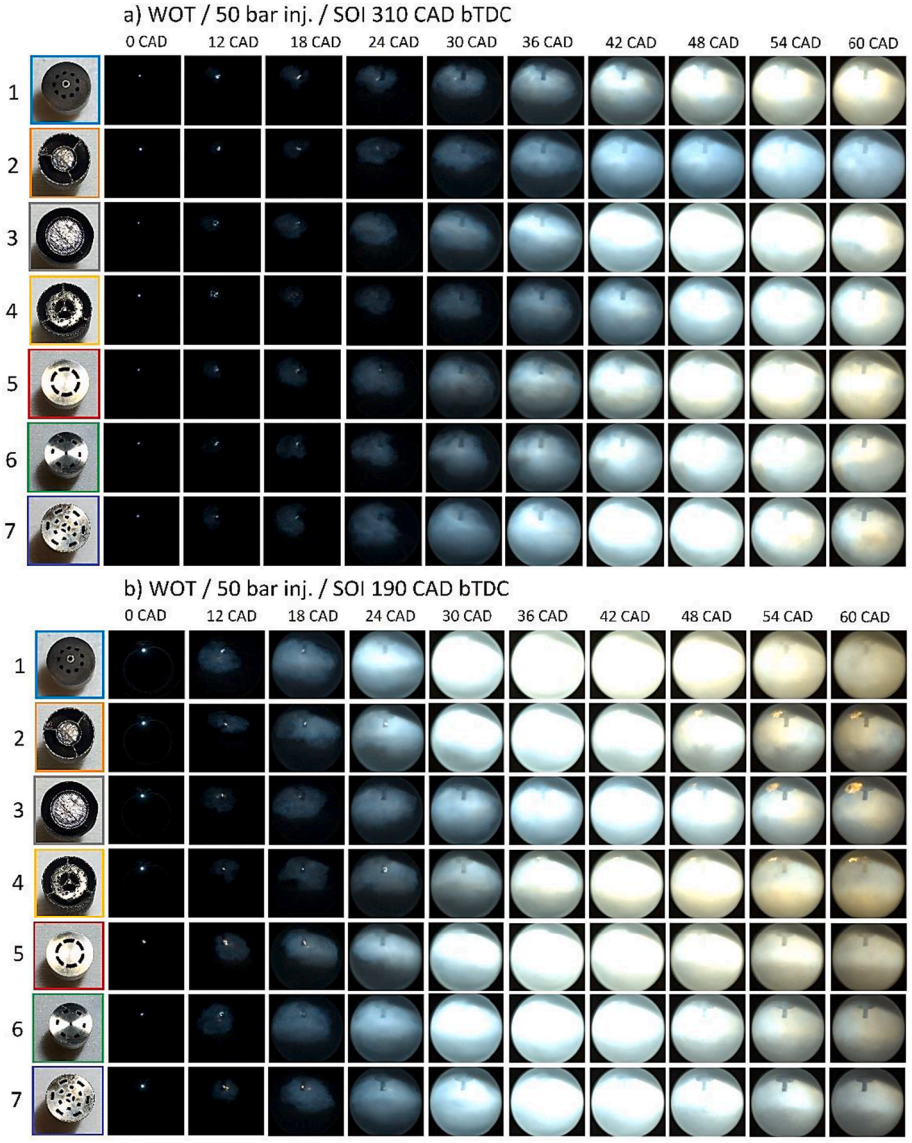

Fig. 16. Combustion process images for different injector nozzle heads at 310 CAD bTDC and 190 CAD bTDC injection timing. WOT conditions, 50 bar injection pressure.

less fuel-rich areas in the cylinder, which can act as sources of yellow flame and particulate formation. However, still small areas of yellow flame around the injector nozzles were detected for nozzle head designs 2, 3 and 4. This finding supported the total PN (Fig. 13c) measurements where the levels of particulate emissions were still higher for mentioned nozzles compared to nozzle heads 1, 5, 6 and 7.

Increasing the injection pressure also increases turbulence in the cylinder, which can improve the combustion process. Combustion images of late injection timing from 18 bar (Fig. 15b) and 50 bar injection pressure (Fig. 16b) showed that the flame developed faster for 50 bar injection pressure mainly with all nozzle heads. This supports the CA10-90 results (Fig. 7c), which showed that CA10-90 values were lower for increased injection pressure and late timing, corresponding to a shorter combustion duration.

Other research groups have also reported that late injection timings with high injection pressure achieved a larger flame radius that was likely enhanced by a high turbulence intensity, affecting the flame speed and flame propagation direction [16].

As it was mentioned above, the investigation showed that yellow flame appeared in particular tested cases and it correlated with increased total PN (Fig. 13) and iSHC (Fig. 11) emission levels. Presented combustion images (Figs. 14-16) represented just single combustion cycles for each nozzle head just for two SOI timings. Further investigation and presented Fig. 17 involved frequency analysis of yellow flame from ~60 combustion cycles (captured ~20 cycles for 3 repetitions) for each nozzle head design and all tested cases.

A relative frequency of 0 means that there were 0 combustion cases with a yellow flame source and 1 means that all combustion cycles had a yellow flame. Investigated cases clearly show that yellow flame trends in the combustion cycles correlate with total PN measurements (Fig. 13). The more combustion cycles included yellow flame, the more total PN levels increased. Nozzle heads 2, 3 and 4 showed one of the highest yellow flame frequencies for both engine loads – 6 bar IMEP (Fig. 17a) and WOT (Fig. 17b and c). Also, the yellow flame started to appear more frequently for other nozzle types when the SOI timing was retarded and frequency values increased sharply when SOI reached 130–190 CAD bTDC depending on the specific case. Relatively frequency results revealed that nozzle head design can have a great impact on reducing fuel-rich zones and yellow flame formation even at earlier SOI timing, e.g SOI at 250 CAD bTDC either for 6 bar IMEP, either for WOT cases.

Fig. 18 represents combustion images for all 7 nozzle heads tested at 6 bar IMEP engine load and the latest SOI timings where the PN levels

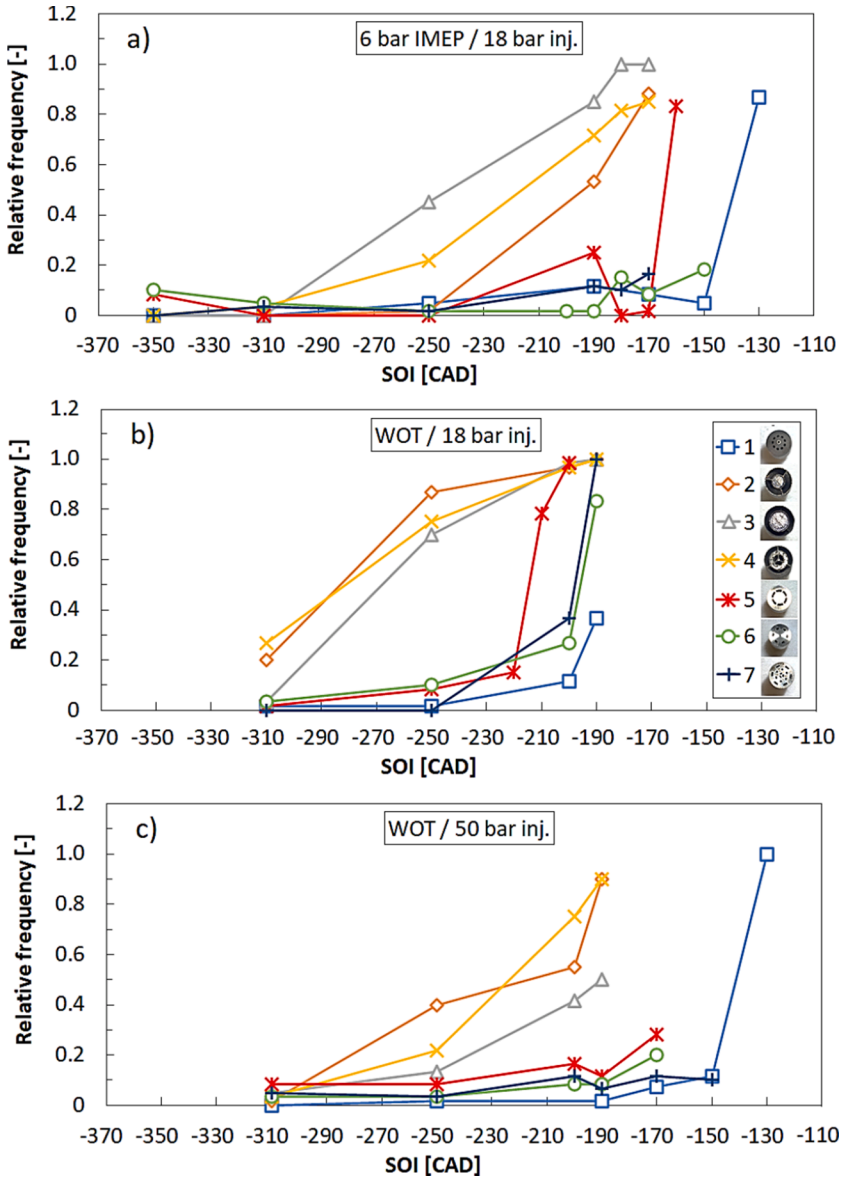

Fig. 17. Relative frequency of yellow flame appearance from 60 combustion cycles for different injector nozzle heads at different SOI timings and injection pressures.

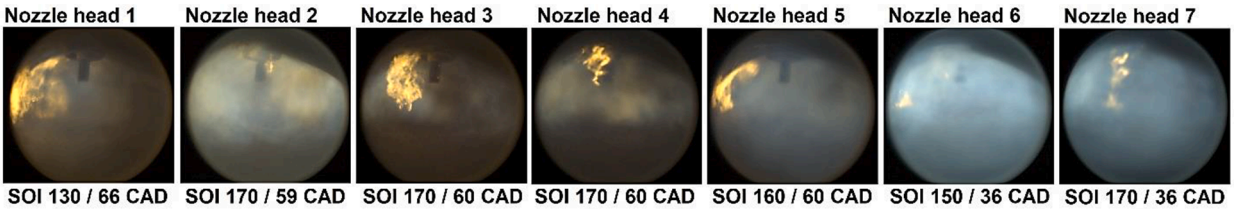

Fig. 18. Combustion process images for different injector nozzle heads at the latest tested SOI timing and particular timing after the ignition. 6 bar IMEP, 18 bar injection pressure.

were the highest. Combustion images were selected to show a more detailed view of yellow flame formation in specific areas depending on nozzle head type.

Analysis showed that yellow flame formation area in the cylinder and timing can differ depending on nozzle head design. Pool fires of yellow flame were mostly observed at the left side of the visual endoscope area for nozzle heads 1, 5 and 6 – at the exhaust valves and a cylinder wall. This was created by fuel rich zones which were sources of higher soot formation, increased PN levels and unburned hydrocarbons. The formation of pool fires at the cylinder wall or exhaust valves was also likely

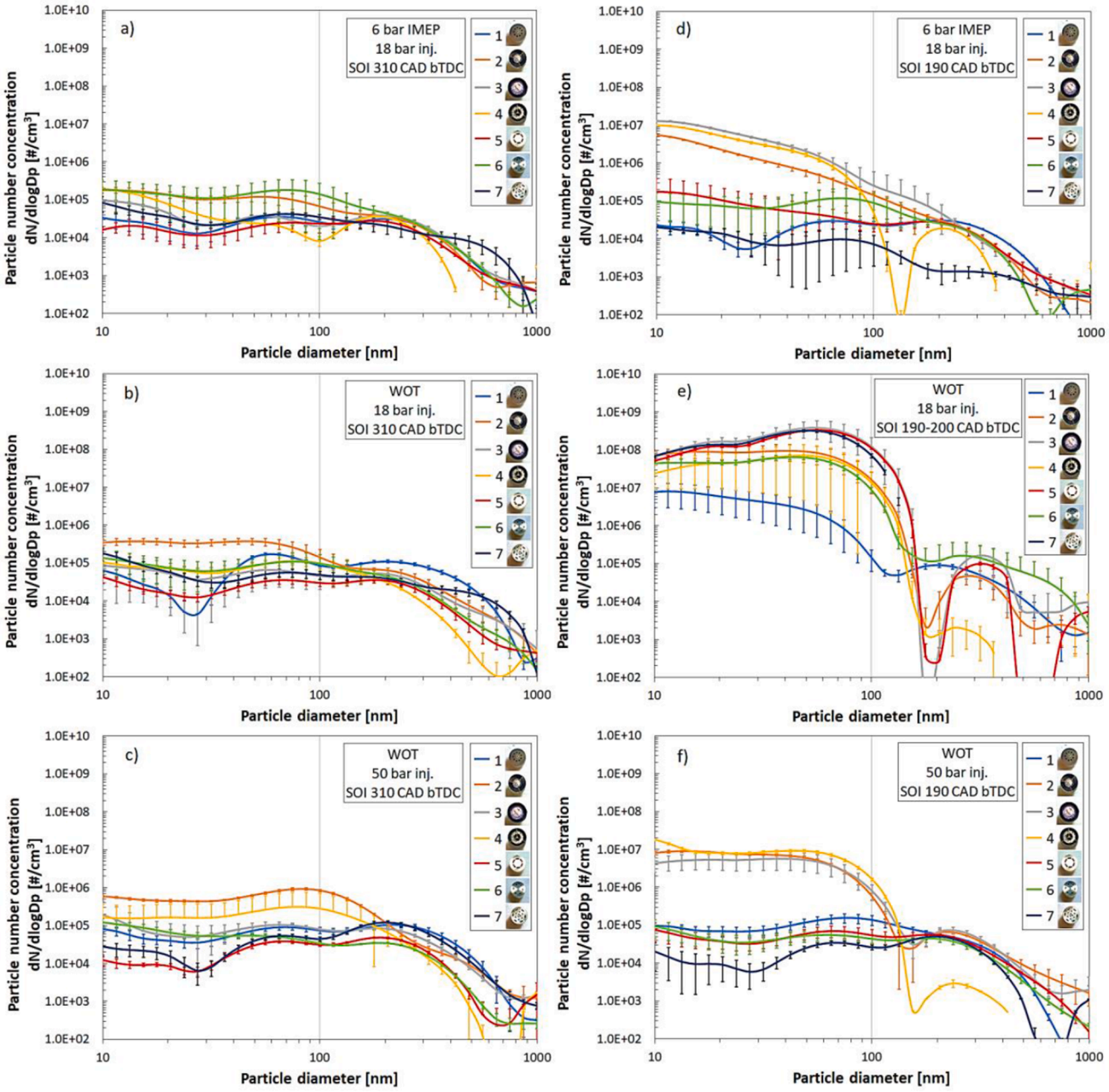

Fig. 19. Particle size distribution for different injector nozzle heads at different SOI timings, engine loads and injection pressures.

to be influenced by the turbulence in the cylinder and combustible mixture motion towards these areas. However, pool fires of yellow flame from mentioned nozzle heads were detected just at very late SOI timing (130–170 CAD bTDC) depending on nozzle head type. Also, the timing of yellow flame appearance after the ignition differed depending on the nozzle head. Pool fires from nozzle heads 6 and 7 were observed much earlier (~36 CAD after the ignition) compared to nozzle heads 3, 4, 5 (~60 CAD after the ignition). As discussed before, yellow flame and soot formation at earlier timing are more preferable as it can be easier oxidized due to higher temperatures at earlier combustion phase.

Achieving good air/fuel mixing and high stoichiometry in the whole cylinder is a challenging but very important criterion. If the fuel-rich zones are appearing at the cylinder walls it is more complicated to oxidize the soot. Researchers noted that soot was formed at the flame front and it was reduced by oxidation at high temperatures with a sufficient time. The oxidation rates were highest at the center of the cylinder and lowest at the cylinder wall due to changes in local temperatures and OH concentrations [56].

Analysis of combustion images from nozzle heads 3 and 4 showed that pool fires and diffusion burn type flame appeared mostly at the injector location at the later combustion phase. Also, images revealed that yellow flame was forming at two locations for the nozzle head 2 – at the injector nozzle head tip and at the spark plug crevices. This proves that large crevices either at the nozzle head, either at the spark plug should be avoided if the fuel is injected at the compression phase as it can be a possible cause of fuel-rich region formation and increased soot emissions. Other research studies also observed that the engine efficiency and some emissions may be affected by the electrode length and size of crevices in the spark plug [69].

3.4. Particle size distribution

Fig. 19 presents the particle size distribution for different nozzle types under 6 bar (18 bar injection pressure) and WOT conditions (18 bar and 50 bar injection pressures). The plots include just two SOI timing conditions – early injection at 310 CAD bTDC (Fig. 19a–c) and late injection at 190–200 CAD bTDC (depending on nozzle type) (Fig. 19d, e and f). These points were chosen so that all nozzle heads could be compared at the same SOI for all tested load conditions. The particle size distribution and concentrations are presented on a logarithmic scale together with error bars representing the standard deviation for different particle size points.

The analysis showed that at SOI of 310 CAD, the highest concentration of particles was at size 10–30 nm for most of the nozzle heads at part load (Fig. 19a) and WOT (Fig. 19b and c). It is known that 10–23 nm size particles represent nucleation (nuclei) mode particles. Larger particles than 23 nm represent accumulation mode particles which are formed by the growth of nuclei particles and their coagulation. Broadly spherical particles are particularly formed when combustion temperature decreases [70]. It is also known that nuclei particles are more volatile organic compounds (VOCs) which are mainly unburnt or partially burnt fuel or have a footprint of lubricants (oil) [71]. The present study showed that at SOI 310 CAD bTDC the highest particle concentration of nuclei particles peaked between ~1.5×10^4 #/cm^3 and ~7×10^5 #/cm^3 depending on the nozzle type and engine load conditions. Higher levels of nuclei particles are likely to be the result of methane characteristics to form smaller particles as mentioned before. Also, smaller particles might be formed due to the VOCs – unburned fuel or lubricant. Fig. 19b and c show that nozzle heads 2 and 4 emitted higher levels of nuclei particles compared to other nozzle heads. The comparison of iSHC emissions (Fig. 11b and c) for the same nozzle heads 2 and 4 also showed slightly higher hydrocarbon levels meaning that combustion efficiency was lower and more unburned fuel was emitted which might be a cause of increased soot emissions and higher levels of smaller particles. Some peaks at 70–300 nm were also observed, which are specific for accumulation mode particles. Higher levels of accumulation particles were detected under high load WOT conditions both at 18 bar and 50 bar injection pressure (Fig. 19b and c). As it was mentioned before, accumulation particles are formed at the later combustion phase when combustion temperature decreases and nuclei particles coagulate into larger size particles (70–100 nm). At later phase particles collide with each other and agglomerate. The agglomeration process can be influenced by thermal or turbulent processes [72].

For a later injection timing of 190 CAD bTDC and 6 bar IMEP load point (Fig. 19d), the particle number concentration peaks for nozzle heads 1, 4, 5, 6 and 7 were in the range $2x10^4$-$2x10^5$ #/cm^3 and the peaks corresponded to either nuclei or accumulation mode sizes. However, nozzle heads 2, 3 and 4, which have larger crevices, showed increased PN emissions and nuclei mode particles reached levels of ~5×10^6–1.5×10^7#/cm^3 (Fig. 19d). Combustion images and analysis of yellow flame relative frequency proved that these nozzle heads tend to form fuel-rich zones which led to pool fires with yellow flame in the majority of combustion cycles. At later injection timing the combustion temperature was lower which reduced the soot oxidation process. Decreased combustion temperature can be proved by reduced iSNO$_x$ emission levels (Fig. 12a) at the same SOI timing – 190 SOI bTDC. It is well known that NO$_x$ formation is very much dependent on oxygen amount and combustion temperature.

Under increased load conditions (WOT) and at 18 bar injection pressure, total PN levels increased for all nozzle heads at late injection timing (190–200 CAD bTDC) (Fig. 13b). This was also evident in the particle size distribution plot (Fig. 19e), which showed that the PN concentration increased for all the tested nozzle types, peaking at ~8×10^7–4×10^8 #/cm^3 level. The peaks correspond to either nuclei or accumulation mode ranges. However, the majority of the nozzle heads (except nozzle head 1) showed the highest level of accumulation mode particles. As discussed before, the time to mix methane gas with air was too short at late injection timing. Thus, fuel-rich zones were created. Yellow flame's relative frequency (Fig. 17b) showed that almost all combustion cycles had pool fires of yellow flame due to low local stoichiometry and low combustion efficiency. This created a high level of soot formation and PN. Reduction in combustion efficiency and combustion stability (Fig. 6b) also reduced combustion temperature which led to lower iSNO$_x$ emissions (Fig. 12b), together with increased iSHC emissions (Fig. 11b). Lower combustion temperature worsened the oxidation process of PAHs which are cause to form soot and soot precursors. Also, the iSFC (Fig. 8b) increased at late SOI timing, therefore more fuel was injected and resulted in even more soot and particulate formation. As mentioned before reduction in combustion temperature resulted in increased accumulation mode particle formation when nuclei mode particles coagulated.

A different trend in particle size distribution at WOT and at late SOI was observed when the injection pressure was increased to 50 bar (Fig. 19f). Nozzle heads 1, 5, 6 and 7 showed a reduction of PN concentration in the nuclei mode range when the pressure was increased from 18 bar to 50 bar, with the highest levels in the range ~3×10^4–2×10^5 #/cm^3, similar to those measured at 6 bar IMEP load. However, increasing the injection pressure did not reduce the PN concentration for nozzle heads 2, 3 and 4, which peaked at ~5×10^6–9×10^6 #/cm^3 in both the nuclei and accumulation mode ranges. Again, these results can be supported by the yellow flame analysis because nozzle heads 2, 3 and 4 were the only ones to show pool fires or diffusion burn type flames (Fig. 17c) at SOI 190 CAD bTDC compared to other nozzle heads. This shows that nozzle heads with smaller crevices or having multiple holes are more preferable than nozzle heads with larger crevices at increased fuel injection pressure and late injection timing to reduce soot and particulate formation.

It was concluded that the DI-CNG injector nozzle type can have a large influence on PN formation when a late injection timing is applied. The use of a higher injection pressure may be a solution to improve combustion and decrease soot formation. However, in some cases, additional improvements in injector nozzle head design may be

necessary to achieve better air/fuel mixing.

4. Conclusions

Experimental investigation of inwards opening and spray-guided DI-CNG injector in a 4-stroke spark ignition engine showed that engine performance and exhaust gas emission parameters can be influenced by the design of injector nozzle head. The obtained results were also highly dependent on the fuel injection pressure and injection timing. Thus, gaseous fuel DI injector nozzle heads should be designed carefully so that they work efficiently while some of the engine control parameters can vary. The main findings and conclusions of the present study can be summarized as follows:

1. Injector nozzle heads with multiple holes/orifices and reduced dead volumes showed improved combustion stability and duration at late injection timing under part load and high load conditions when the fuel was injected at 18 bar injection pressure. Nozzle heads with smaller crevices achieved higher maximum IMEP under WOT conditions. Increasing the injection pressure to 50 bar led to no major differences in the combustion parameters between the nozzle heads. A higher injection pressure increased the combustion stability, the engine achieved higher engine load and extended the possibility of injecting at later timing for all injector nozzle heads compared to at 18 bar injection pressure.
2. Emissions of $iSCO_2$, iSCO and iSHC were higher for the injector nozzle heads with larger crevices at part load or WOT and 18 bar injection pressure. Increased emissions remained from early to late injection timing. At the same tested load and injection pressure, iSCO and iSHC showed an increasing trend for all injector nozzle heads at late injection timing, which was attributed to incomplete air/fuel mixing and changed combustion efficiency. At both loads and 18 bar injection pressure, emission levels of $iSNO_x$ decreased for all injector nozzle head types at late injection timing due to reduced combustion efficiency and combustion temperature. Increasing the injection pressure to 50 bar improved the combustion process and combustion stability and decreased $iSCO_2$, iSCO and iSHC emissions levels at late injection timing for all nozzle types. However, $iSNO_x$ emissions increased for all DI injector nozzle heads at late injection timing due to increased turbulence in the cylinder and an improved combustion process enabled by the higher fuel injection pressure.
3. Total PN levels only slightly varied among the different injector nozzle head types and just blue flame formation was dominant at an early injection timing (310 CAD bTDC). Total PN started to increase earlier at later injection timing (250 CAD bTDC) for the nozzle heads with the larger crevices. However, all nozzle heads showed increased total PN by several orders of magnitude when the fuel was injected at 18 bar and very late injection timing either at part load or WOT. Increased particulate levels were mainly related to reduced time available for air/fuel mixing, formation of fuel-rich zones in the cylinder and decreased timing to oxidize the soot. Combustion images proved that yellow flame was present in the cylinder at late injection timings and its frequency in the combustion cycles was correlating with increased total PN levels meaning that yellow flame formation was a dominant source for soot in the pool fires. Increasing the injection pressure under WOT conditions improved total PN levels at late injection timing. Higher injection pressure increased turbulence in the cylinder and improved combustion duration. The lowest PN levels were achieved with the nozzle heads having multiple holes, most likely because they could spread the fuel concentration over a wider volume with smaller jets and achieve higher air/fuel homogeneity. The formation of yellow flame also reduced which led to a lower soot formation.
4. The highest peaks of particle size were found to be in the broad range of 10 to 300 nm for all nozzle head types under various testing conditions when the fuel was injected early, i.e., 310 CAD bTDC. At a late injection timing of 190 CAD bTDC, nuclei mode particles with diameters of 10–30 nm were dominant for the most nozzle head types at part load. At WOT, 18 bar injection pressure and late injection timing the nuclei particles also tended to form more together with accumulation particles. High levels of nuclei and accumulation particles formation correlated with iSHC emissions and it was mainly related to low local stoichiometry in the cylinder and unburned fuel. Accumulation mode particles formed at the later combustion phase due to reduced combustion temperature and coagulating nuclei particles. Increasing the injection pressure to 50 bar reduced the formation of nuclei and accumulation mode particles for the nozzle types having multiple holes. In contrast, nozzle heads with large crevices still showed higher PN levels at late injection timing due to the formation of fuel-rich areas.
5. Combustion image analysis of different injector nozzle heads showed that blue flame formation was dominant at an early injection timing (310 CAD bTDC), part load or WOT conditions and 18 bar or 50 bar injection pressure. Under the latter conditions, a yellow flame was visible in the cylinder for all injector nozzle head designs, which correlated with increased PN levels. Yellow flame formation area in the cylinder and timing differed depending on nozzle head design. Pool fires of yellow flame were more detected at cylinder walls for nozzle heads with multiple holes and the same type of flame observed in the vicinity of the spark plug or injector tip for nozzles having larger crevices. Increasing the injection pressure to 50 bar at WOT improved the air/fuel mixing and reduced the chances of yellow flame formation, decreasing the formation of particulates.

Declaration of Competing Interest

The authors declare the following financial interests/personal relationships which may be considered as potential competing interests: The research was funded by “Swedish Energy Agency” (Project number P44829-1). The financial support from “Swedish Energy Agency” was also acknowledged in the paper. Also, authors acknowledged the technical support from GDTech Engineering company during the DI-CNG injector tests.

Acknowledgments

We gratefully acknowledge financial support from the Swedish Energy Agency (Project number P44829-1). We also acknowledge personnel at GDTech Engineering for providing valuable hardware and support about the DI-CNG injection system.

References

[1] European Commission. Communication from the Commission. The European Green Deal. 11.12.2019. Accessed on 2021 July. Available on: https://eur-lex.europa.eu/legal-content/EN/TXT/?uri=COM%3A2019%3A640%3AFIN.
[2] European Commission. Electrification of the Transport System. Studies and Reports. Accessed on 2020 April. Available on: https://ec.europa.eu/programmes/horizon2020/en/news/electrification-transport-system-expert-group-report -0.
[3] Yontar AA, Dogu Y. Effects of equivalence ration and CNG addition of engine performance and emissions in a dual sequential ignition engine. International J of Engine Research 2019;1–16, IMechE. https://doi.org/10.1177/1468087419834190.
[4] Napolitano P, Alfˆe M, Guido C, Gargiulo V, Fraioli V, Beatrice C. Particle emissions from HD SI gas engine fueled with LPG and CNG. Fuel 2020;269:117439. 10.1016/j.fuel.2020.117439.
[5] Duc KN, Duy VN, Hoang-Dinh L, Viet TN, Le-Anh T. Performance and emission characteristics of a port fuel injected, spark ignition engine fueled by compressed natural gas. Sustainable Energy Technol Assess 2019;31:383–9. https://doi.org/10.1016/j.seta.2018.12.018.
[6] Jahirul MI, Masjuki HH, Saidur R, Kalam MA, Jayed MH, Wazed MA. Comparative engine performance and emission analysis of CNG and gasoline in a retrofitted car engine. Appl Therm Eng 2010;30(14-15):2219–26. https://doi.org/10.1016/j.applthermaleng.2010.05.037.
[7] Thiruvengadam A, Besch MC, Yoon S, Collins J, Kappanna H, Carder DK, et al. Characterization of Particulate Matter Emissions from a Current Technology Natural Gas Engine. Environ. Sci. Technol. 2014;48(14):8235–42. https://doi.org/10.1021/es5005973.

[8] Bielaczyc P, Woodburn J, Szczotka A. Particulate Emissions from European Vehicles Featuring Direct Injection Spark Ignition Engines Tested Under Laboratory Conditions. SAE Int. J. Fuels Lubr 2014;7(2):580–90. https://doi.org/10.4271/2014-01-1608.

[9] Guido, C., Fraioli, V., Napolitano, P., Alfuso, Sew. et al., "Emissive Behavior of a Heavy-Duty SI Gas Engine During WHTC," SAE Technical Paper 2019-24-0121, 2019, https://doi.org/10.4271/2019-24-0121.

[10] Toumasatos Z, Kontses A, Doulgeris S, Samaras Z, Ntziachristos L. Particle Emissions Measurements on CNG Vehicles Focusing on Sub-23nm. Aerosol Sci Technol 2020;55(2):182–93. https://doi.org/10.1080/02786826.2020.1830942.

[11] Singh AP, Pal A, Agarwal AK. Comparative particulate characteristics of hydrogen, CNG, HCNG, gasoline and diesel fueled engines. Fuel 2016;185:491–9. https://doi.org/10.1016/j.fuel.2016.08.018.

[12] Baratta M, Misul D, Xu J. Development and application of a method for characterizing mixture formation in a port-injection natural gas engine. Energy Convers Manage 2021;227:113595. https://doi.org/10.1016/j.enconman.2020.113595.

[13] Lee J, Park C, Bae J, Kim Y, Lee S, Kim C. Comparison between gasoline direct injection and compressed natural gas port fuel injection under maximum load condition. Energy 2020;197:117173. https://doi.org/10.1016/j.energy.2020.117173.

[14] Sankesh D, Edsell J, Mazlan S, Lappas P. Comparative study between early and late injection in a natural-gas fuelled spark-ignited direct-injection engine. Energy Procedia 2017;110:275–80. https://doi.org/10.1016/j.egypro.2017.03.139.

[15] Hagos FY, Aziz ARA, Sulaiman SA, Firmansyah, Mamat R. Effect of fuel injection timing of hydrogen rich syngas augmented with methane in direct-injection spark-ignition engine. Int J Hydrogen Energy 2017;42(37):23846–55. https://doi.org/10.1016/j.ijhydene.2017.03.091.

[16] Chen L, Wei H, Zhang R, Pan J, Zhou L, Liu C. Effects of late injection on lean combustion characteristics of methane in a high compression ratio optical engine. Fuel 2019;225:115718. https://doi.org/10.1016/j.fuel.2019.115718.

[17] Aljamali S, Abdullah S, Mahmood WMFW, Ali Y. Effect of fuel injection timings on performance and emissions of stratified combustion CNGDI engine. Appl Therm Eng 2016;109:616–29. https://doi.org/10.1016/j.applthermaleng.2016.08.127.

[18] Wu S, Gandhi A, Li H, Meinhart M. Experimental and numerical study of the effect of nozzle taper angle on spray characteristics of GDI multi-hole injectors at cold condition. Fuel 2020;275:117888. https://doi.org/10.1016/j.fuel.2020.117888.

[19] Moon S, Huang W, Wang J. Spray formation mechanism of diverging-tapered-hole GDI injector and its potentials for GDI engine applications. Fuel 2020;270:117519. https://doi.org/10.1016/j.fuel.2020.117519.

[20] Gong C, Zhang Z, Sun J, Chen Y, Liu F. Computational study of nozzle spray-line distribution effects on stratified mixture formation, combustion and emissions of a high compression ratio DISI methanol engine under lean-burn condition. Energy 2020;205:118080. https://doi.org/10.1016/j.energy.2020.118080.

[21] Yamaguchi, A., Koopmans, L., Helmantel, A., Dillner, J. et al., "Spray Behaviors and Gasoline Direct Injection Engine Performance Using Ultrahigh Injection Pressures up to 1500 Bar," *SAE Int. J. Engines* 15(1):2022, 10.4271/03-15-01-0007.

[22] Bartolucci L, Cordiner S, Mulone V, Scarcelli R, Wallner T, Swantek AB, et al. Gaseous jet through an outward opening injector: Details of mixing characteristics and turbulence scales. Int J Heat Fluid Flow 2020;85:108660. https://doi.org/10.1016/j.ijheatfluidflow.2020.108660.

[23] Hamzehloo A, Aleiferis PG. Large eddy simulation of highly turbulent under-expanded hydrogen and methane jets for gaseous-fuelled internal combustion engines. Int J Hydrogen Energy 2014;39(36):21275–96. https://doi.org/10.1016/j.ijhydene.2014.10.016.

[24] Hamzehloo A, Aleiferis PG. Numerical modelling of transient under-expanded jets under different ambient thermodynamic conditions with adaptive mesh refinement. Int J Heat Fluid Flow 2016;61:711–29. https://doi.org/10.1016/j.ijheatfluidflow.2016.07.015.

[25] Yosri MR, Ho JZ, Meulemans M, Talei M, Gordon RL, Brear MJ, et al. Large-eddy simulation of methane direct injection using the full injector geometry. Fuel 2021;290:120019. https://doi.org/10.1016/j.fuel.2020.120019.

[26] Deshmukh A.Y., Bode M., Falkenstein T., Khosravi M., van Bebber D., Klaas M., Schröder W., Pitsch H. Simulation and modeling of direct gas injection through poppet-type outwardly-opening injectors in internal combustion engines. Springer Singapore, Singapore 2019:65–115. 10.1007/978-981-13-3307-1_ 4.

[27] Sankesh D, Petersen P, Lappas P. Flow characteristics of natural-gas from an outward-opening nozzle for direct injection engines. Fuel 2018;218:188–202. https://doi.org/10.1016/j.fuel.2018.01.009.

[28] Montanaro A, Allocca L, De Vita A, Ranieri S, et al. Experimental and Numerical Characterization of High-Pressure Methane Jets for Direct Injection in Internal Combustion Engines. SAE Technical Paper 2020–01-2124, 2020,. https://doi.org/10.4271/2020-01-2124.

[29] Zhao J, Liu W, Grekhov L. Visualization research on influence of ambient pressure on CNG jet characteristics of gas injector with outward-opening nozzle. Fuel 2019;257:116084. https://doi.org/10.1016/j.fuel.2019.116084.

[30] Swantek AB, Duke DJ, Kastengren AL, Sovis N, Powell CF, Bartolucci L, et al. An experimental investigation of gas fuel injection with X-ray radiography. Exp Therm Fluid Sci 2017;87:15–29. https://doi.org/10.1016/j.expthermflusci.2017.04.016.

[31] Keskinen K, Kaario O, Nuutinen M, Vuorinen V, Künsch Z, Liavåg LO, et al. Mixture formation in a direct injection gas engine: Numerical study on nozzle type, injection pressure and injection timing effects. Energy 2016;94:542–56. https://doi.org/10.1016/j.energy.2015.09.121.

[32] Yadollahi B, Boroomand M. The effect of combustion chamber geometry on injection and mixture preparation in a CNG direct injection SI engine. Fuel 2013;107:52–62. https://doi.org/10.1016/j.fuel.2013.01.004.

[33] Chitsaz I, Saidi MH, Mozafari AA, Hajialimohammadi A. Experimental and numerical investigation on the jet characteristics of spark ignition direct injection gaseous injector. Appl Energy 2013;105:8–16. https://doi.org/10.1016/j.apenergy.2012.11.023.

[34] Zoldak P, Naber J. Spark Ignited Direct Injection Natural Gas Combustion in a Heavy Duty Single Cylinder Test Engine – Start of Injection and Spark Timing Effects. SAE Technical Paper 2015–01-2813 2015. https://doi.org/10.4271/2015-01-2813.

[35] Seboldt D, Lejsek D, Wentsch M, Chiodi M, et al. Numerical and Experimental Studies on Mixture Formation with an Outward-Opening Nozzle in a SI Engine with CNG-DI. SAE Technical Paper 2016–01-0801, 2016,. https://doi.org/10.4271/2016-01-0801.

[36] Catapano, F., Di Iorio, S., Sementa, P., and Vaglieco, B., "Particle Formation and Emissions in an Optical Small Displacement SI Engine Dual Fueled with CNG DI and Gasoline PFI," SAE Technical Paper 2017-24-0092, 2017, 10.4271/2017- 24-0092.

[37] Hofmann P, Hofherr T, Hoffmann G, Preuhs JF. Potential of CNG Direct Injection for Downsizing Engines. MTZ Worldwide 2016;77(7–8):28–35. https://doi.org/10.1007/s38313-016-0074-6.

[38] Seboldt D., Lejsek D., Bargende M. Experimental study on the impact of the jet shape of an outward-opening nozzle on mixture formation with CNG-DI. Internationales Stuttgarter Symposium, Proceedings, 2016, 459-477, doi 10.1007/978-3-658-13255-2_95.

[39] Vuorinen V, Wehrfritz A, Duwig C, Boersma BJ. Large-eddy simulation on the effect of injection pressure and density on fuel jet mixing in gas engines. Fuel 2014;130:241–50. https://doi.org/10.1016/j.fuel.2014.04.045.

[40] Farzaneh-Gord M, Arabkoohsar A, Koury RNN. Novel natural gas molecular weight calculator equation as a functional of only temperature, pressure and sound speed. J Nat Gas Sci Eng 2016;30:195–204.

[41] McTaggart-Cowan G, Huang J, Munshi S. Impacts and Mitigation of Varying Fuel Composition in a Natural Gas Heavy-Duty Engine. SAE Int. J. Engines 2017;10(4):1506–17. https://doi.org/10.4271/2017-01-0777.

[42] Melaika M, Herbillon G, Dahlander P. Spark ignition engine performance, standard emissions and particulates using GDI. PFI-CNG and DI-CNG systems. Fuel 2021;293:120454. https://doi.org/10.1016/j.fuel.2021.120454.

[43] Melaika M, Mamikoglu S, Dahlander P. 48V Mild-Hybrid Architecture Types, Fuels and Power Levels Needed to Achieve 75g CO2/km. SAE Technical Paper 2019–01-0366, 2019,. https://doi.org/10.4271/2019-01-0366.

[44] Heywood, J.B., "Internal Combustion Engine Fundamentals," McGraw-Hill: p. 960, 1988, ISBN-10: 007028637X.

[45] Mohammed S.E., Baharom M.B., Aziz A.R.A., Firmansyah. The effects of fuel-injection timing at medium injection pressure on the engine characteristics and emissions of a CNG-DI engine fueled by a small amount of hydrogen in CNG. International Journal of Hydrogen Energy 36 (2011) 11997-12006, doi:10.1016/j.ijhydene.2011.05.110.

[46] Moon S. Potential of direct-injection for the improvement of homogeneous-charge combustion in spark-ignition natural gas engines. Appl Therm Eng 2018;136:41–8. https://doi.org/10.1016/j.applthermaleng.2018.01.068.

[47] Song J., Choi M., Kim D., Park S. Combustion Characteristics of Methane Direct Injection Engine Under Various Injection Timings and Injection Pressures. Journal of Engineering for Gas Turbines and Power. 2017 August, Vol. 139/8 p.

[48] Choi M, Song J, Park S. Modeling of the fuel injection and combustion process in a CNG direct injection engine. Fuel 2016;179:168–78. https://doi.org/10.1016/j.fuel.2016.03.099.

[49] Seboldt D, Lejsek D, Bargende M. Injection strategies for low HC raw emissions in SI engines with CNG direct injection. Automot. Engine Technol. 2016;1:81–91. https://doi.org/10.1007/s41104-016-0002-4.

[50] Sevik James, Pamminger Michael, Wallner Thomas, Scarcelli Riccardo, Boyer Brad, Wooldridge Steven, et al. Influence of Injector Location on Part-Load Performance Characteristics of Natural Gas Direct-Injection in a Spark Ignition Engine. SAE Int. J. Engines 2016;9(4):2262–71. https://doi.org/10.4271/2016-01-2364.

[51] Bartolucci L, Cordiner S, Mulone V, Rocco V. Natural Gas Fueled Engines Modeling under Partial Stratified Charge Operating Conditions. SAE Technical Paper 2017–24-0093, 2017,. https://doi.org/10.4271/2017-24-0093.

[52] Zeng Ke, Huang Zuohua, Liu Bing, Liu Liangxin, Jiang Deming, Ren Yi, et al. Combustion characteristics of a direct-injection natural gas engine under various fuel injection timings. Appl Therm Eng 2006;26(8-9):806–13. https://doi.org/10.1016/j.applthermaleng.2005.10.011.

[53] Baratta M, Rapetto N. Mixture Formation Analysis in a Direct-Injection NG SI Engine Under Different Injection Timings. Fuel 2015;159:675–88. https://doi.org/10.1016/j.fuel.2015.07.027.

[54] Hora TS, Shukla PC, Agarwal AK. Particulate emissions from hydrogen enriched compressed natural gas engine. Fuel 2016;166:574–80. https://doi.org/10.1016/j.fuel.2015.11.035.

[55] Adlercreutz L, Cronhjort A, Stenlaas O. Particle Emission Measurements in a SI CNG Engine Using Oils with Controlled Ash Content. SAE Technical Paper 2019–01-0053, 2019,. https://doi.org/10.4271/2019-01-0053.

[56] Amirante R, Distaso E, Tamburrano P, Reitz R. Measured and Predicted Soot Particle Emissions from Natural Gas Engines. SAE Technical Paper 2015–24-2518, 2015,. https://doi.org/10.4271/2015-24-2518.

[57] Melaika M, Andersson M, Dahlander P. Methane Direct Injection in an Optical SI Engine – Comparison between Different Combustion Modes. SAE Technical Paper 2019–01-0083 2019. https://doi.org/10.4271/2019-01-0083.

[58] Liu Yu, Yeom Jeongkuk, Chung Seongsik. A study of spray development and combustion propagation processes of spark-ignited direct injection (SIDI)

compressed natural gas (CNG). Math Comput Modell 2013;57(1-2):228–44. https://doi.org/10.1016/j.mcm.2011.06.035.
[59] Stojkovic BD, Fansler TD, Drake MC, Sick V. High-Speed Imaging of OH* and Soot Temperature and Concentration in a Stratified-Charge Direct-Injection Gasoline Engine. Proceedings of theCombustion Institute 2005;30:2657–65. https://doi.org/10.1016/j. proci.2004.08.021.
[60] An Y, Teng S, Pei Y, Qin J, Li X, Zhao H. An experimental study of polycyclic aromatic hydrocarbons and soot emissions from a GDI engine fueled with commercial gasoline. Fuel 2016;164:160–71. https://doi.org/10.1016/j.fuel.2015.10.007.
[61] Gong C, Sun J, Liu F. Numerical study of twin-spark plug arrangement effects on flame, combustion and emissions of a medium compression ratio direct-injection methanol engine. Fuel 2020;279:118427. https://doi.org/10.1016/j.fuel.2020.118427.
[62] Karavalakis Georgios, Hajbabaei Maryam, Jiang Yu, Yang Jiacheng, Johnson Kent C, Cocker David R, et al. Regulated, greenhouse gas, and particulate emissions from lean-burn and stoichiometric natural gas heavy-duty vehicles on different fuel compositions. Fuel 2016;175:146–56. https://doi.org/10.1016/j.fuel.2016.02.034.
[63] Glassman, I. and Yetter, R.A., Combustion Fourth Edition (Elsevier, 2008), 773. ISBN:978-0-12-088573-2.
[64] Bartok W, Kuriskin RJ. Formation of Soot Precursors in Diffusion Flames. Combust Sci Technol 1988;58(4–6):281–95. https://doi.org/10.1080/00102208808923968.
[65] Merola Simona Silvia, Marchitto Luca, Tornatore Cinzia, Valentino Gerardo, Irimescu Adrian. UV-Visible Optical Characterization of the Early Combustion Stage in a DISI Engine Fuelled with Butanol- Gasoline Blend. SAE Int. J. Engines 2013;6(4):1953–69. https://doi.org/10.4271/2013-01-2638.
[66] Glassman, I., "Soot Formation in Combustion Processes," Symposium (International) on Combustion 22(1):295-311, 1989, doi:10.1016/S0082-0784(89)80036-0.
[67] Haynes, B.S. and Wagner, H.G., "Soot Formation," Progress in Energy and Combustion Science 7:229-273, 1981, doi:10.1016/0360-1285(81)90001-0.
[68] Tree Dale R, Svensson Kenth I. Soot Processes in Compression Ignition Engines. Prog Energy Combust Sci 2007;33(3):272–309. https://doi.org/10.1016/j.pecs.2006.03.002.
[69] Park C., Kim C., Choi Y., Lee S. Effect of spark plug protrusion on the performance and emission characteristics of an engine fueled by hydrogen-natural gas blends. Journal of Mechanical Science and Technology 28 (4) (2014) 1539-1544, doi 10.1007/s12206-014-0140-4.
[70] Raza M, Chen L, Leach F, Ding S. A Review of Particulate Number (PN) Emissions from Gasoline Direct Injection (GDI) Engines and Their Control Techniques. Energies 2018;11(6):1–26. https://doi.org/10.3390/en11061417.
[71] Hu Naitao, Tan Jianwei, Wang Xiaoyan, Zhang Xuemin, Yu Peng. Volatile organic compound emissions from an engine fueled with an ethanol-biodiesel-diesel blend. J Energy Inst 2017;90(1):101–9. https://doi.org/10.1016/j.joei.2015.10.003.
[72] Überall A, Otte R, Eilts P, Krahl J. A literature research about particle emissions from engines with direct gasoline injection and the potential to reduce these emissions. Fuel 2015;147:203–7. https://doi.org/10.1016/j.fuel.2015.01.012.